Electronic Supplementary Information (ESI)

Strain-triggered acidification in a double-network hydrogel enabled by multi-functional transduction of molecular mechanochemistry

Tetsu Ouchi,‡ Brandon H. Bowser,‡ Tatiana B. Kouznetsova, Xujun Zheng and Stephen L. Craig*

‡These authors contributed equally to this work

*Corresponding author: stephen.craig@duke.edu

Contents

1. General Information

1.1. Materials

All solvents (chloroform, hexane, ethyl acetate, acetone, tetrahydrofuran, toluene) were purchased from either Sigma-Aldrich or VWR. Toluene was purified with an Innovative Technology solvent purification system. nButyl acrylate and 2-(Methacryloyloxy)ethyl acetoacetate were purchased from Sigma-Aldrich and purified through a plug of basic alumina prior to use. 2-Acrylamido-2-methyl-1-propanesulfonic acid sodium salt (NaAMPS) solution 50 wt.% in H_2O was purchased from Sigma-Aldrich. 2-Acrylamido-2-methyl-1-propanesulfonic acid sodium salt was purified as follows: it was first precipitated in Acetone, then cooled in a fridge overnight, any precipitate was then collected via filtration and dried under high vacuum. All other chemicals were purchased from Sigma-Aldrich or Matrix Scientific and used without further purification. For all small molecule synthesis, the flasks were flame dried before the reactions. Flash chromatography was performed with Silicycle SiliaFlash® F60 gel (40-63 μm particle size, 230-400 mesh), and medium pressure liquid chromatography (MPLC) was performed with a CombiFlash Rf 200 (Teledyne ISCO).

1.2. Characterization

^{1}H (proton), ^{13}C (c13cpd), and 2D ^{1}H-^{13}C-HMQC (hmqcgp) NMR experiments were conducted on a Bruker Avance 500 MHZ with a iprobe; ^{1}H-HOMODEC measurements were performed with a 500 MHz Varian UNITY spectrometer with a HFCN probe; 2D ^{1}H-^{1}H-NOESY (noesyph) was conducted on a Bruker Avance 700 MHz with a BBO probe. All NMR experiments were conducted at room temperature. The residual solvent peaks were used as an internal reference peak for chemical shifts ($CDCl_3$: 7.26 ppm [^{1}H], 77.16 ppm [^{13}C]). Chemical shifts are reported in ppm (δ), multiplicity, coupling constants (J) in Hz (if applicable), and relative integral. Multiplicity is given as singlet (s), doublet (d), triplet (t), quartet (q), multiplet (m), or broad (b).

High-resolution mass spectrometry was conducted with an Agilent LCMS-TOF-DART at the Mass Spectrometry Facility at Duke University.

Gel permeation chromatography (GPC) was performed with two in-line Agilent PLgel mixed-C columns (10^5 Å, 7.5 x 300 mm, 5 μm, part number PL1110-6500) with a flow rate of 1.0 mL/min of THF eluent stabilized with 100 ppm 3,5-Di-tert-4-butylhydroxytoluene (BHT) inhibitor. Molecular weights were determined by using a Wyatt Optilab T-rEX refractive index detector and Wyatt miniDAWN TREOS multiangle light scattering (MALS) detector with the refractive index increment (dn/dc), which was calculated by 100% mass recovery assumption based on the injection volume and the known concentration. UV spectra were measured with Agilent 1260 Infinity UV detector. All samples were prepared in a THF solution with a concentration of 2 mg/ml and were filtered through a PTFE syringe filter with a 0.2 μm pore size.

Sonication experiments were conducted by a Sonics Vibracell Model VCX750 at 20 kHz with a 13 mm diameter probe at 0 °C using an ice bath. The amplitude was set as 30%, and the sonication sequence was set as 1 s on and 1 s off. The sonication samples were prepared in THF with a concentration of 2 mg/ml.

UV-vis measurements were performed with a Photonics Model 440 UV-Vis Spectrophotometer.

Tensile test and cyclic test were conducted using a Dynamic Mechanical Analyzer (DMA) from TA Instruments, specifically the RSA III model at Duke University's Shared Materials Instrumentation Facility (SMIF). The strain speed was set as 10 %strain/s.

The AFM pulling experiments were carried out using a homemade AFM, similar to the one described in detail previously,[1] in toluene at an ambient temperature (~23˚C) using the same protocol as described before.[2–6] Sharp Microlever silicon probes (MSNL) were obtained from Bruker (Camarillo, CA), and the force curves used for analysis were acquired using rectangular-shaped cantilevers (205 µm x 15 µm, nominal tip radius ~2 nm, nominal spring constant k ~ 0.02 N/m, frequency ~15 kHz). Cantilever spring constants were calibrated in air using the thermal noise method, based on the energy equipartition theorem, as described previously.[7] Silicon surfaces were prepared by soaking ~30 min in hot piranha solution, followed by washing with copious amounts of DI-water and drying under a stream of nitrogen. Probes were prepared by soaking in piranha solution for ~15 min at room temperature, washing with DI water, and gently drying with Kimwipe. The surface and probe were then placed in a UVO cleaner (Jelight model 42) for 15 min. After ozonolysis, 10-20 µL of a ~0.1-0.05 mg/ml polymer solution was added to the silicon surface and allowed to dry. Measurements were carried out in a fluid cell with scanning set for a series of constant velocity approaching/retracting cycles at 300 nm/s. During acquisition data were filtered with a 500 Hz lowpass filter. Force curves were collected in dSPACE (dSPACE Inc., Wixom, MI) and Matlab (The MathWorks, Inc., Natick, MA) and analyzed later using Matlab.

2. Synthetic procedures

2.1. Synthesis of small molecules

2.1.1. General synthesis procedure of 7,7-dichloro-1,3-dimethoxybicyclo[4.1.0]hept-3-ene

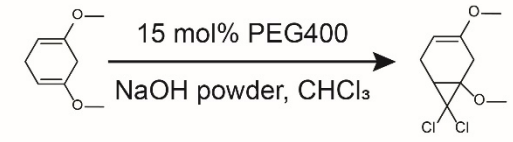

The synthesis of methoxy substituted *gem*-dichlorocyclopropane (MeO-*g*DCC) was conducted with a similar procedure to previously reported methods.[8,9]

1,5-Dimethoxy-1,4-cyclohexadiene (5 g, 35.7 mmol) and PEG400 (*M*n = 400 g/mol, 2.14 g, 5.35 mmol) were dissolved into 150 ml of chloroform in a flame dried flask. The solution was cooled to 0 ˚C with an ice bath and kept for 10 – 15 min. Then, sodium hydroxide powder (2.14 g, 53.5 mmol) was slowly added to the solution, and the flask was removed from the ice bath. After being stirred for 30 min at room temperature, 100 - 200 ml of diethyl ether was added, and the insoluble solids were filtered. The filtrate was washed with 1 M HCl (1 x 150 ml), DI water (5 x 150 ml), and Brine (1 x 150 ml). The organic phase was then dried over magnesium sulfate and filtered. The solvent was removed under reduced pressure, and an oily product (8.53 g) was obtained. The product was used for the subsequent reaction without further purification. If the product had magnesium sulfate residues, it was dissolved in anhydrous toluene (10 ml) and filtered through 5 µm pore size PTFE syringe filter for the subsequent reaction.

2.1.2. General synthesis procedure of compound 1

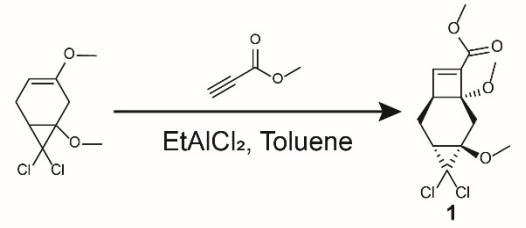

Compound **1** was synthesized using a similar procedure to previously reported methods.[10–12]

To a flame dried flask under nitrogen, anhydrous toluene (46.9 ml) was added. Ethylalmumium dichloride in toluene (25 wt%, 25.1 ml of the solution, 45.9 mmol of ethylalmunium dichloride) was slowly added, followed by the slow addition of methyl propiolate (4.18 g, 44.7 mmol). To the solution, sparged 7,7-dichloro-1,3-dimethoxybicyclo[4.1.0]hept-3-ene (8.53 g, 38.2 mmol) in anhydrous toluene (10 ml) was slowly added, and the reaction mixture was stirred overnight at room temperature. Then, the reaction mixture was poured into a saturated aqueous solution of $KHPO_4$ (300 ml) and stirred for 20 min. To this solution, 60 ml of 10% HCl aqueous solution was added, followed by extraction with diethyl ether (3 x 300 ml). The combined organic layer was washed with DI water (1 x 300 ml), Brine (1 x 300 ml), dried over sodium sulfate, and filtered. Solvent was removed under reduced pressure, and the residual oil was purified with flash chromatography (SiO_2, Ethyl acetate/Hexane 5% or 0 to 25% gradient elution) to give compound **1** as a slightly yellow solid (2.44 g, total yield for both steps: 22%).

^{1}H NMR (500 MHz, $CDCl_3$) δ 6.88 (d, J = 1.0 Hz, 1H), 3.78 (s, 3H), 3.42 (s, 3H), 3.34 (s, 3H), 2.98-2.97 (m, 1H), 2.88 (dd, J = 15.1, 1.8 Hz, 1H), 2.28-2.22 (m, 1H), 1.83 (d, J = 15.1 Hz, 1H), 1.64 (td, J = 8.8, 1.7 Hz, 1H), 1.52-1.47 (m, 1H).

^{13}C NMR (126 MHz, $CDCl_3$) δ 161.43, 148.47, 140.94, 80.54, 68.96, 66.69, 54.83, 51.96, 51.55, 43.11, 32.71, 25.68, 21.01.

HRMS-ESI (m/z): $[M+H]^+$ calculated for $C_{13}H_{16}Cl_2O_4$ 307.0498, observed 307.0495; $[M+Na]^+$ calculated 329.0318, observed 329.0314.

1D and 2D NMRs were conducted to identify its chemical structure, and their spectra are included as Fig. S1-S5. Specifically, ^{1}H-HOMODEC spectra show a coupling between proton a and e (Fig. S4): the peak associated with proton e is affected under the irradiation at the position of proton a, while the peak associated with proton a changes its shape under the irradiation at the position of proton e. This indicates that cyclobutene methacrylate is installed with methyl ether being with the same side as the two methoxies on the hexane ring. In 2D NOSEY NMR spectrum (Fig. S5), proton c interacts with only proton g, but not with proton h. On the other hand, proton d couples with proton h, but not with g. This suggests that the two methoxies, which have proton c and d, takes anti-position upon the cycloadditions of dichlorocyclopropane and cyclobutene methacrylate.

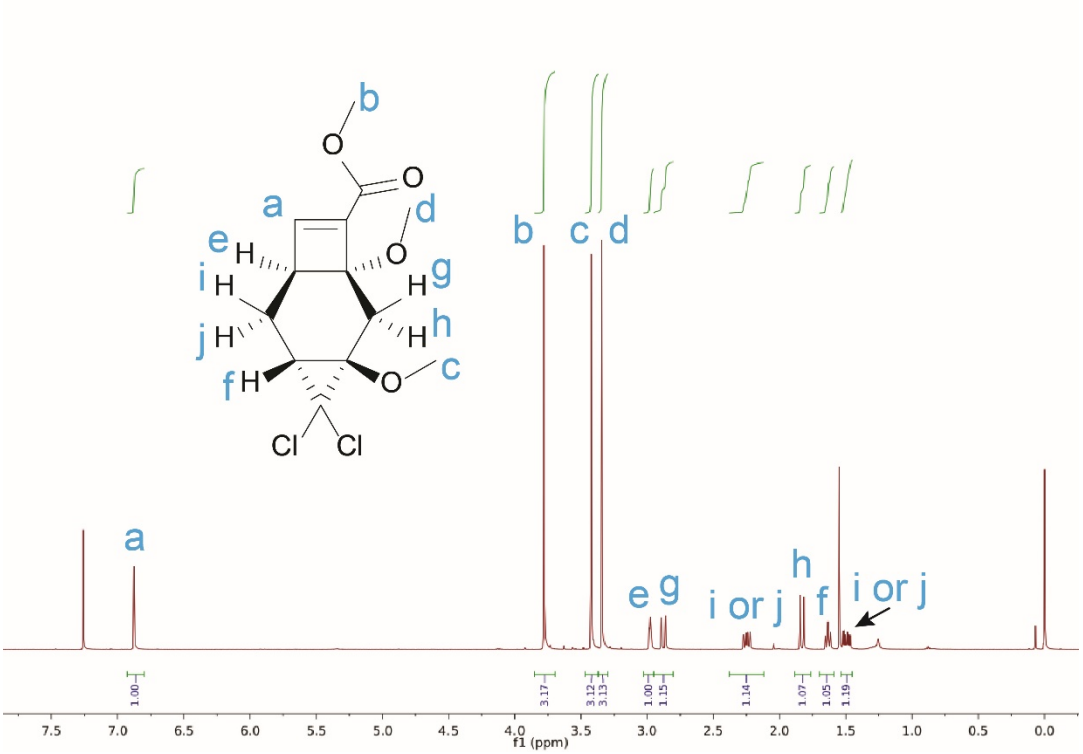

Fig. S1. ^{1}H NMR spectrum of compound **1** (500 MHz, $CDCl_3$)

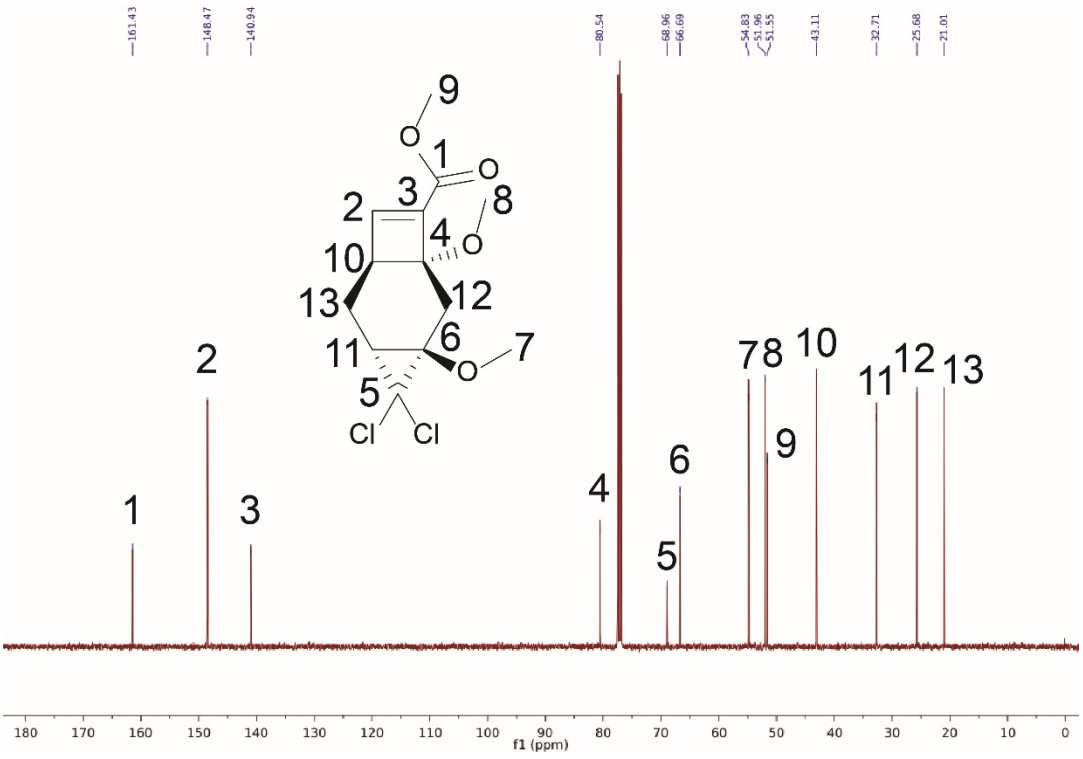

Fig. S2. ^{13}C NMR spectrum of compound **1** (126 MHz, $CDCl_3$)

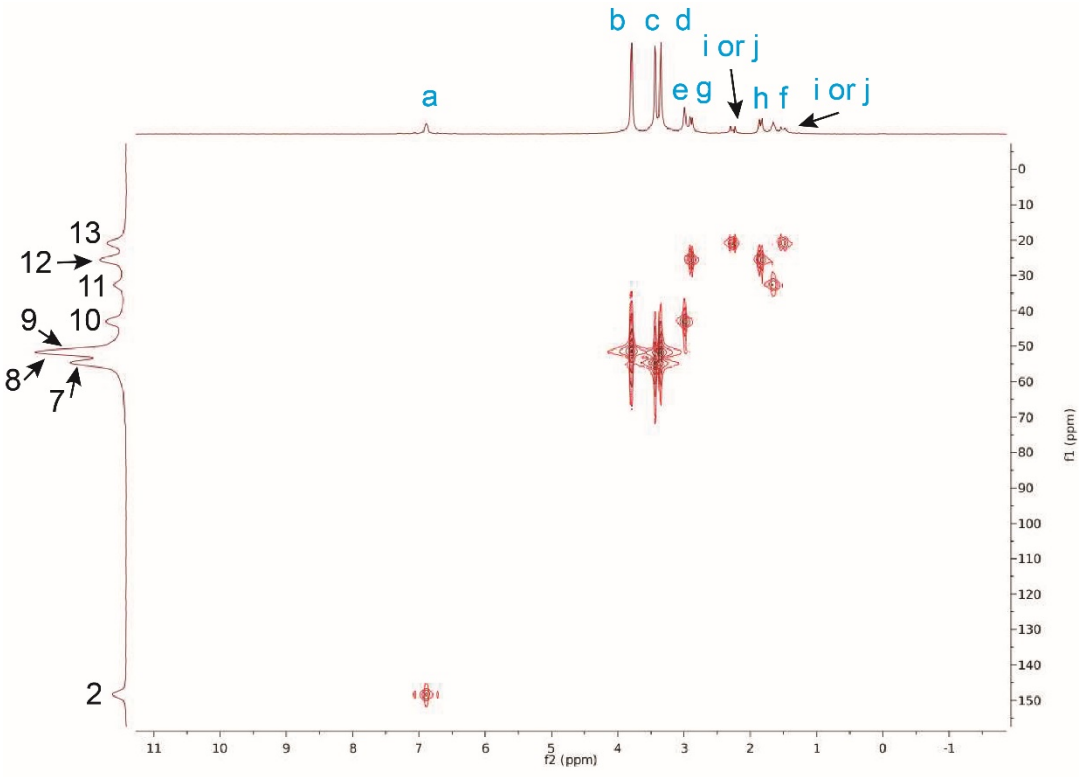

Fig. S3. 2D ^{1}H-^{13}C-HMQC NMR spectrum of compound **1**

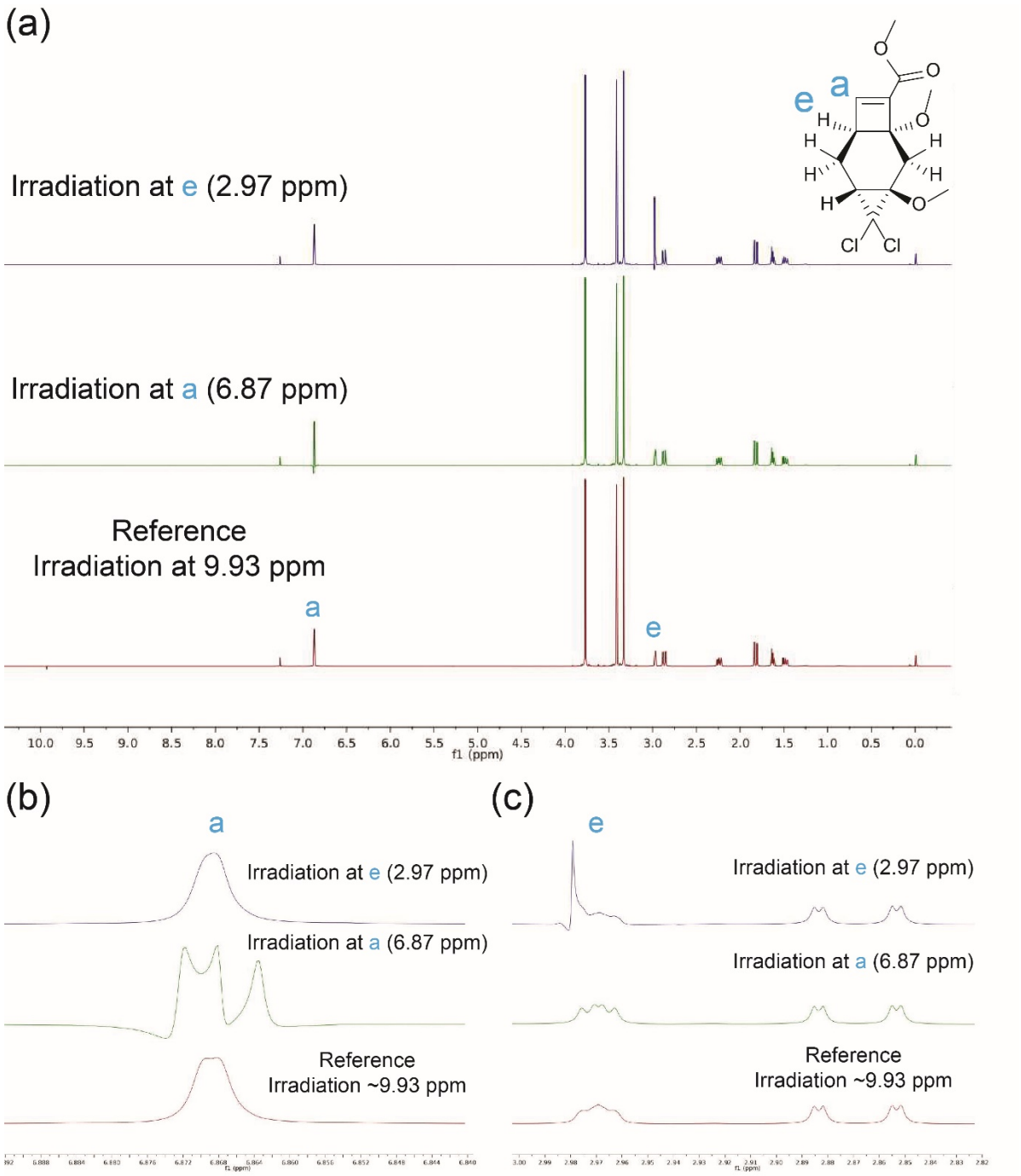

Fig. S4. ^{1}H-HOMODEC NMR spectrum of compound **1**: (a) whole view of the ^{1}H-HOMODEC spectra, (b) magnified spectra around 6.87 ppm, and (c) magnified spectra around 2.97 ppm.

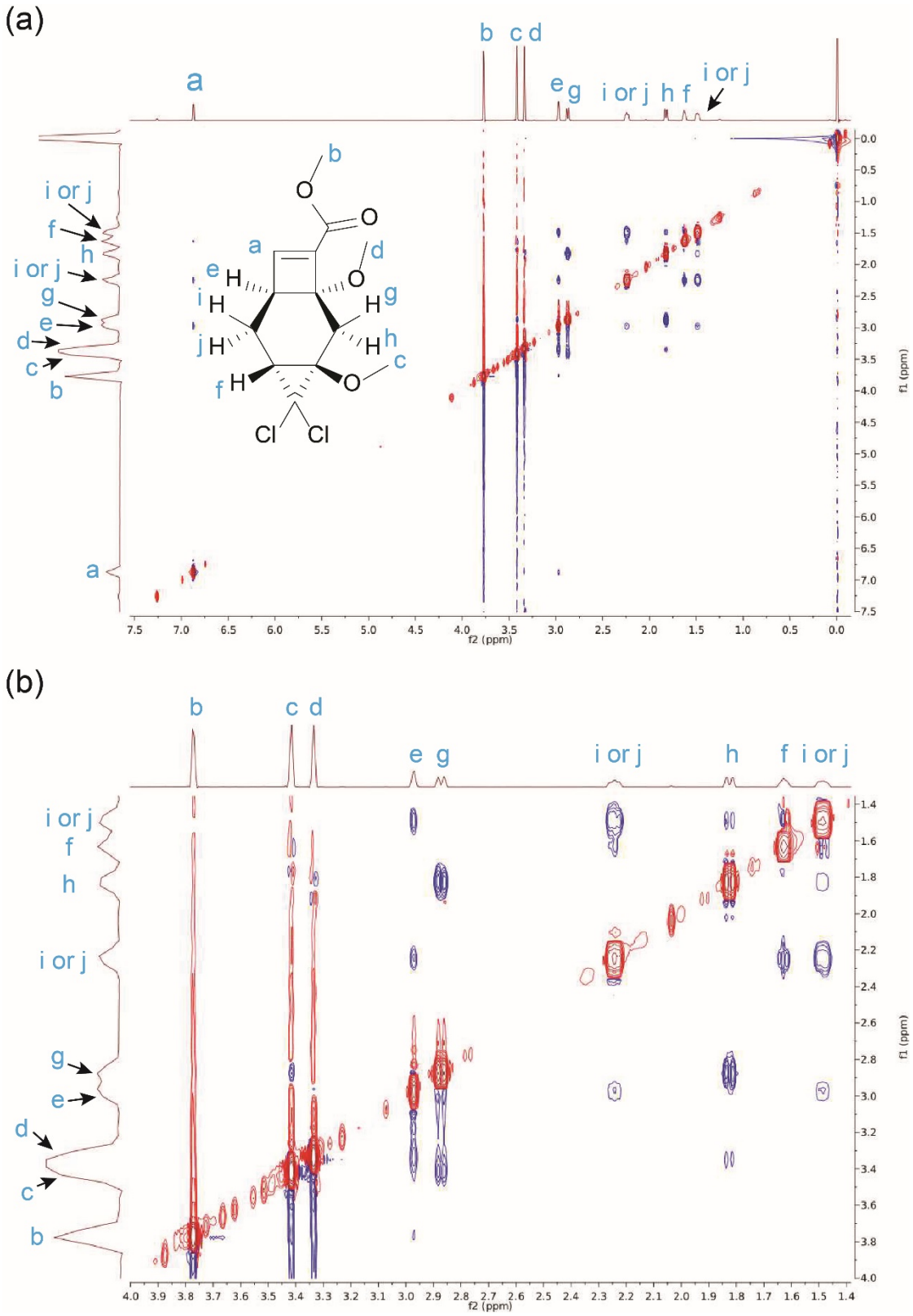

Fig. S5. 2D ^{1}H-^{1}H-NOSEY NMR spectrum of compound **1**: (a) whole 2D spectrum and (b) magnified spectrum.

2.1.3. General synthesis procedure of 7,7-dichloro-1-methoxybicyclo[4.1.0]hept-3-ene

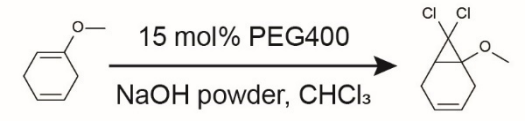

The synthesis of 7,7-dichloro-1-methoxybicyclo[4.1.0]hept-3-ene was conducted using the previously reported procedure.[8]

1-Methoxy-1,4-cyclohexadiene (3 g, 27.2 mmol) and 15 mol% of polyethylene glycol (PEG400: *M*n = 400 g/mol, 1.63 g, 4.08 mmol) were dissolved in chloroform (54.5 ml). The flask was immersed in an ice bath, and the solution was cooled to 0 °C. Then, NaOH powder (3.27 g, 81.7 mmol) was slowly added to the solution, and the flask was warmed up to room temperature. After stirring for 30 min, diethyl ether (200 ml) was added to the solution. The insoluble solids were filtered, and the filtrate was washed with 1 M HCl solution (1 x 75 ml), DI water (5 x 75 ml), and brine (1 x 75 ml). The organic phase was dried over magnesium sulfate and filtered. The solvent was removed under reduced pressure, and an oily product was obtained. The product was used for the subsequent reaction without further purification.

2.1.4. General synthesis procedure of compound 2

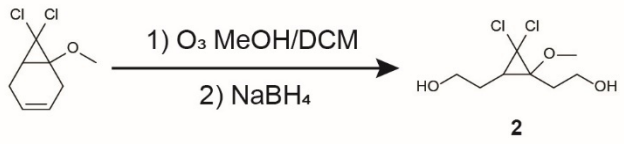

The synthesis of compound **2** was conducted using the previously reported procedure.[8]

7,7-dichloro-1-methoxybicyclo[4.1.0]hept-3-ene (5.26 g, 27.2 mmol) was dissolved in MeOH (54.5 ml) and DCM (27.2 ml) mixture. The solution was cooled to -78 °C, and O_3 was bubbled through the solution. The solution turned purple, and the reaction was monitored with TLC. After the initial materials were consumed, O_2 was bubbled through to remove O_3. Then, $NaBH_4$ (6.3 g, 166.5 mmol) was slowly added to the solution at -78 °C. The mixture was slowly warmed up to room temperature and stirred overnight. After the reaction was completed, MeOH/DCM was removed under reduced pressure, and DI water (150 ml) was added. Then, the mixture was extracted with ethyl acetate (3 x 150 ml), dried over magnesium sulfate, and filtered. The filtrate was dried over SiO_2 under reduced pressure, and the mixture was purified with flash chromatography (Ethyl acetate/Hexane 0 to 100% gradient elution) to give compound **2** as a colorless liquid (4.48 g, total yield for both steps: 72 %).

^{1}H NMR (500 MHz, $CDCl_3$) δ 3.96 – 3.69 (m, 4H), 3.44 (s, 3H), 2.63 (s, 2H), 2.15 (m, 1H), 1.94 (m, 1H), 1.84 – 1.61 (m, 3H).

^{13}C NMR (126 MHz, $CDCl_3$) δ 68.50, 67.43, 61.29, 59.24, 54.91, 37.22, 28.98, 28.23.

HRMS-ESI (m/z): $[M+H]^+$ calculated for $C_8H_{14}Cl_2O_3$ 229.0393, observed 229.0394; $[M+Na]^+$ calculated 251.0212, observed 251.0213.

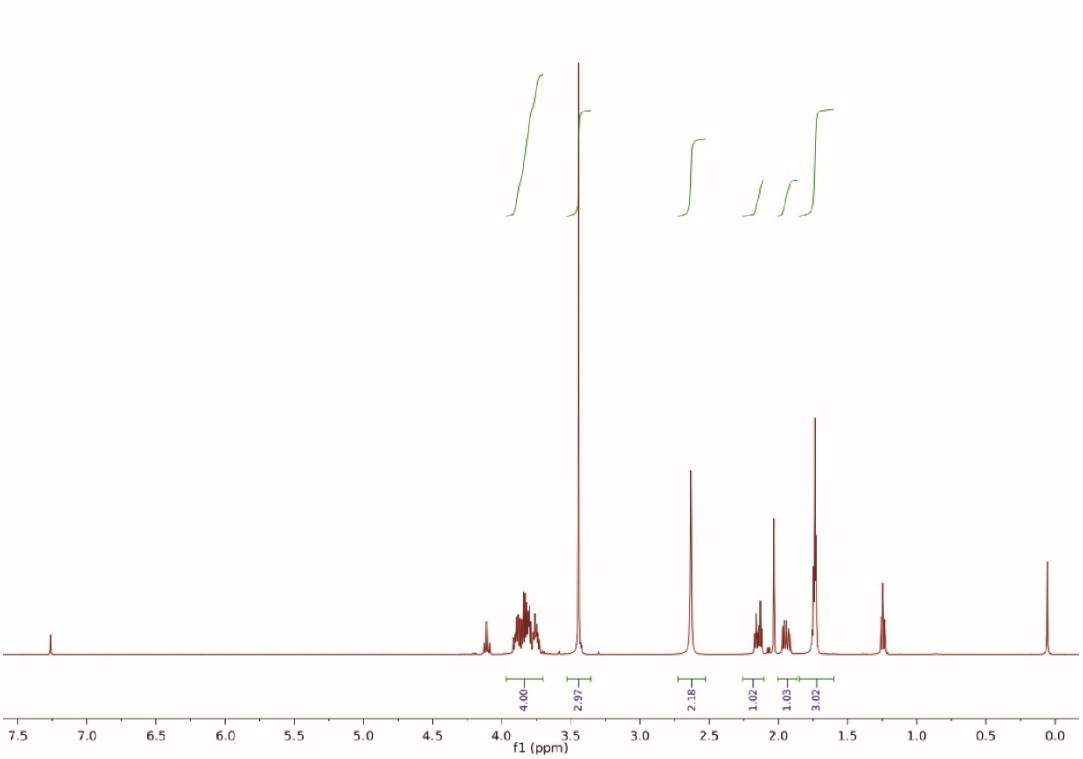

Fig. S6. ^{1}H NMR spectrum of compound **2** (500 MHz, $CDCl_3$)

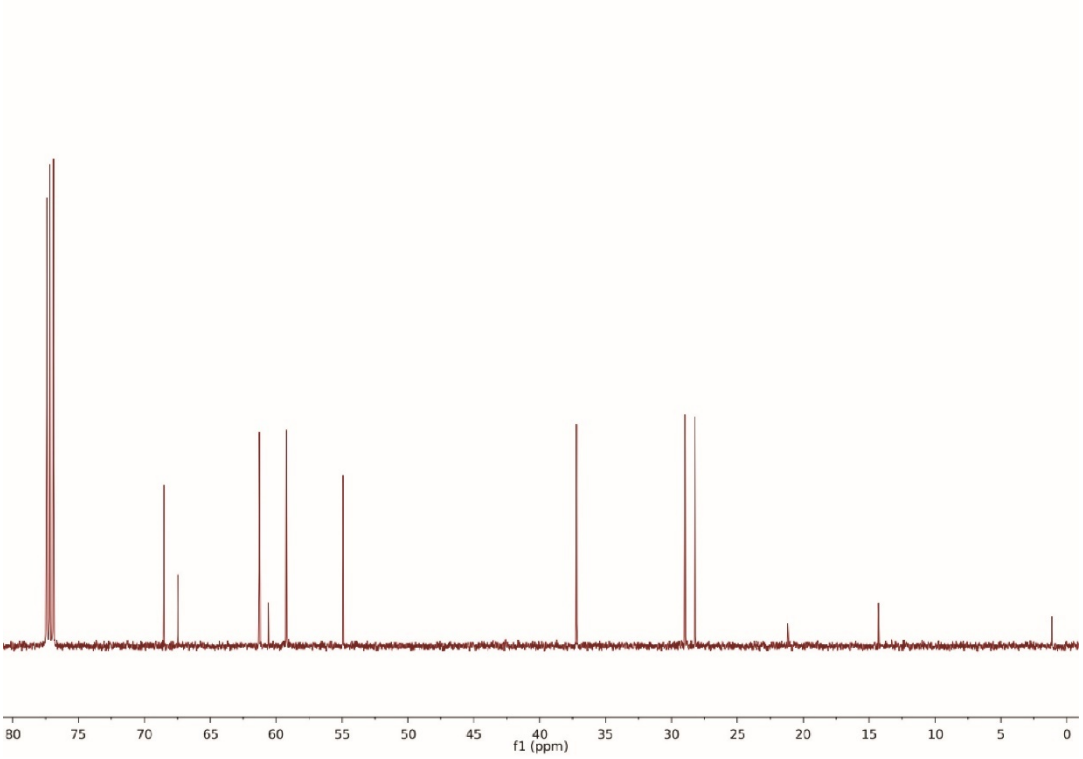

Fig. S7. ^{13}C NMR spectrum of compound **2** (126 MHz, $CDCl_3$)

2.2. General synthesis procedure of linear polymers

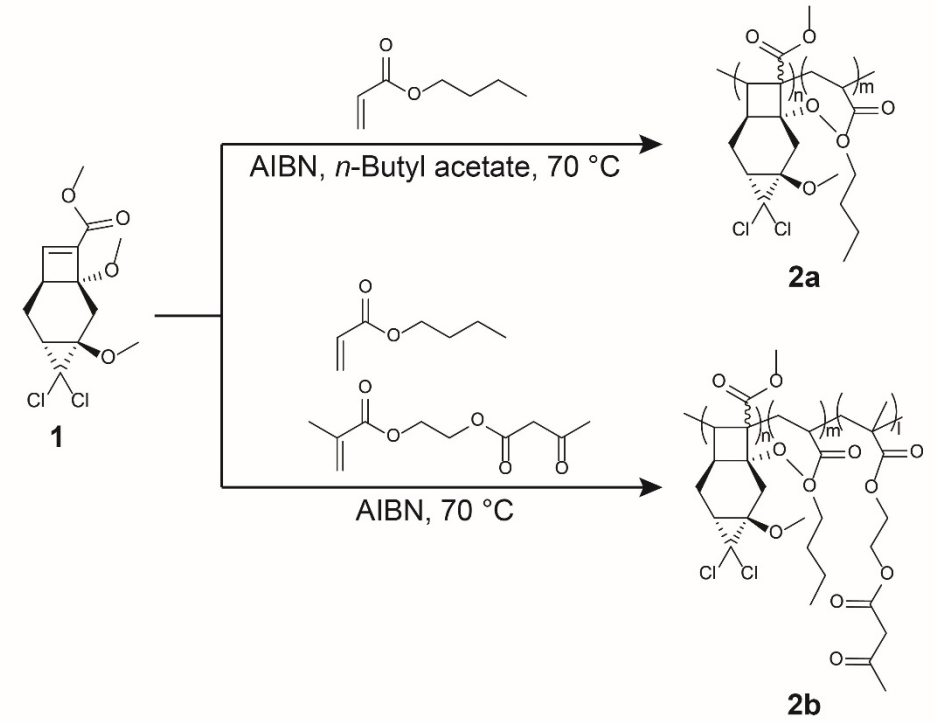

Monomer **1** and its comonomers, 2,2'-azobis(2-methylpropionitrile) (AIBN), and *n*-Butyl acetate (only for sonication) were charged into a flame dried 10 ml Schlenk flask. The mixture was degassed via a minimum of 3 freeze-pump-thaw cycles and then backfilled with nitrogen. Then, the mixture was immersed into an oil bath at 70 ˚C overnight. After the reaction, the mixture was cooled down to room temperature, opened to the air, and precipitated into a cold methanol/DI water mixture (80%/20%) three times. The resulting polymer was dried under vacuum, and its incorporation and molecular weight were characterized by ^{1}H NMR and GPC, respectively. For sonication experiments (**2a**), monomer **1** (52.8 mg, 0.172 mmol), n-butyl acrylate (*n*BA) (51.4 mg, 0.4011 mmol), AIBN (0.732 mg, 0.00446 mmol) and *n*-Butyl acetate (55.3 µl) were used as feed. For SMFS experiments (**2b**), monomer **1** (52.0 mg, 0.169 mmol), *n*-butyl acrylate (163 mg, 1.27 mmol), 2-acetoacetoxyethyl methacrylate (AAEMA) (54.4 mg, 0.254 mmol), AIBN (0.463 mg, 0.00282 mmol) were used as feed, and the polymer was reverse precipitated using methanol.

Copolymer compositions for **2a** and **2b** were calculated using the following equations.[10,11,13]

2a (monomer 1 and *n*BA):

$$Incorporation\ of\ \mathbf{1} = \frac{\frac{A_{blue}}{9}}{(\frac{A_{blue}}{9} + \frac{A_{yellow}}{2})} = \frac{\frac{9.00}{9}}{(\frac{9.00}{9} + \frac{19.41}{2})} = 0.093$$

$$Incorporation\ of\ nBA = \frac{\frac{A_{yellow}}{2}}{(\frac{A_{blue}}{9} + \frac{A_{yellow}}{2})} = \frac{\frac{19.41}{2}}{(\frac{9.00}{9} + \frac{19.41}{2})} = 0.907$$

A_{blue} and A_{yellow} are the areas of 9H (3 methyl) for the gated mechanoacid and 2H (1 methylene) for the *n*BA, respectively.

2b (monomer 1, *n*BA, and AAEMA):

$$Incorporation\ of\ \mathbf{1} = \frac{\frac{A_{blue} - A_{green}}{9}}{(\frac{A_{blue} - A_{green}}{9} + \frac{(A_{yellow} - 2A_{green})}{2} + \frac{A_{green}}{2})}$$

$$= \frac{\frac{3.89 - 2.00}{9}}{(\frac{3.89 - 2.00}{9} + \frac{(12.37 - 2 \times 2.00)}{2} + \frac{2.00}{2})} = 0.039$$

$$Incorporation\ of\ nBA = \frac{\frac{(A_{yellow} - 2A_{green})}{2}}{(\frac{A_{blue} - A_{green}}{9} + \frac{(A_{yellow} - 2A_{green})}{2} + \frac{A_{green}}{2})}$$

$$= \frac{\frac{(12.37 - 2 \times 2.00)}{2}}{(\frac{3.89 - 2.00}{9} + \frac{(12.37 - 2 \times 2.00)}{2} + \frac{2.00}{2})} = 0.775$$

$$Incorporation\ of\ AAEMA = \frac{\frac{A_{green}}{2}}{(\frac{A_{blue} - A_{green}}{9} + \frac{(A_{yellow} - 2A_{green})}{2} + \frac{A_{green}}{2})}$$

$$= \frac{\frac{2.00}{2}}{(\frac{3.89 - 2.00}{9} + \frac{(12.37 - 2 \times 2.00)}{2} + \frac{2.00}{2})} = 0.186$$

A_{green} is the areas of 2H (1 methylene) for AAEMA.

Table S1. The incorporation ratio and the GPC results of the synthesized polymers

	Incorporation ratio[a)]			*Mn*	*Mw*	*Mz*	*Đ*
	Gated mechanoacid	*n*BA	AAEMA	(g/mol)[b)]	(g/mol)[b)]	(g/mol)[b)]	
2a	0.09	0.91	-	64,700	179,000	360,000	2.76
2b	0.04	0.78	0.19	446,000	2,150,000	11,400,000	4.81
2b'	0.04	0.78	0.19	819,000	3,160,000	12,900,000	3.86

[a)] ^{1}H NMR and [b)] GPC-MALS

2b' is **2b** after reverse precipitation. The incorporation ratios for polymer **2b'** is based the incorporation ratio determined prior to the reverse precipitation of polymer **2b**.

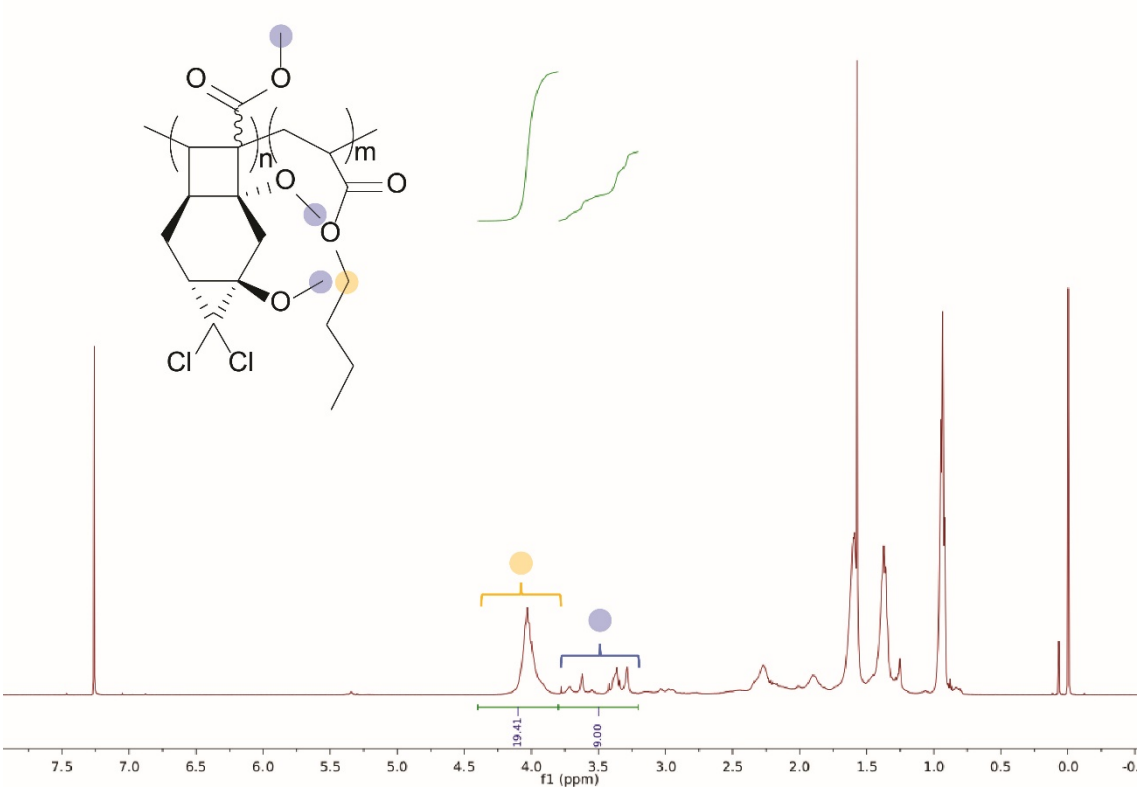

Fig. S8. ^{1}H NMR (500 MHz, $CDCl_3$) spectrum of polymer **2a** for sonication experiment with the integrals used to determine the incorporation ratios of each monomer.

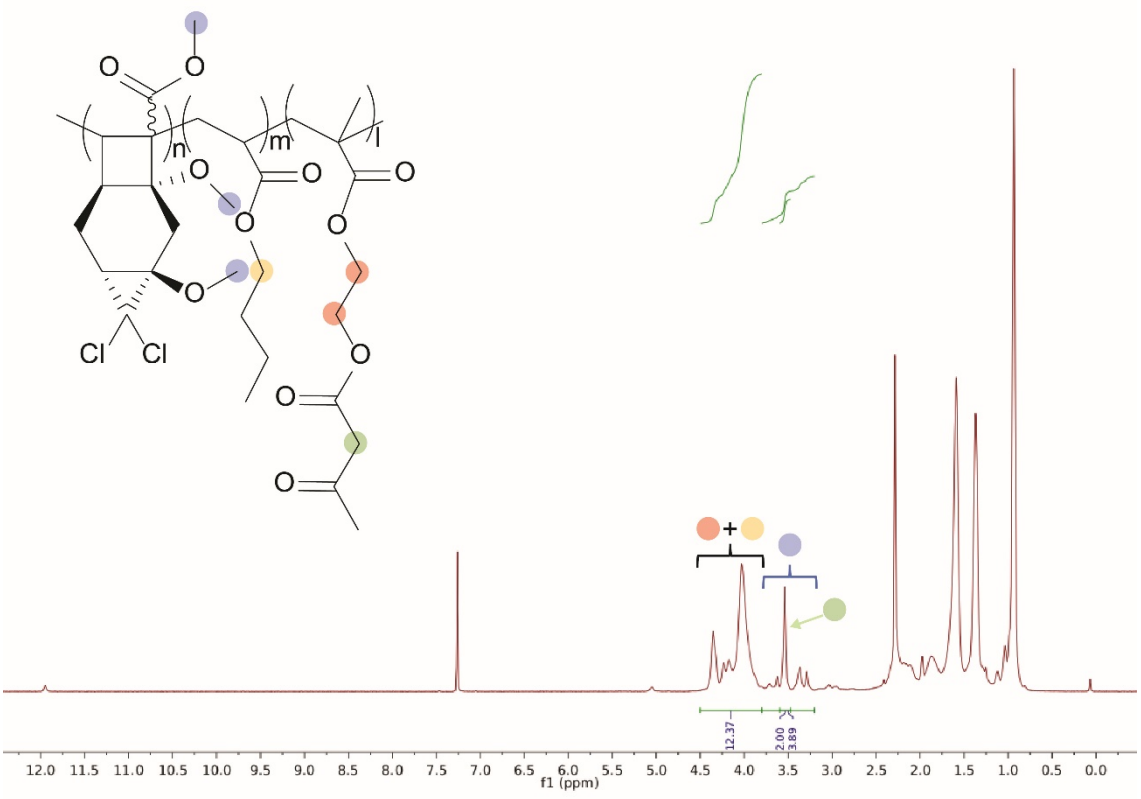

Fig. S9. ^{1}H NMR (500 MHz, $CDCl_3$) spectrum of polymer **2b** for SMFS experiment with the integrals used to determine the incorporation ratios of each monomer.

2.3. General synthesis procedure of the double-network hydrogels

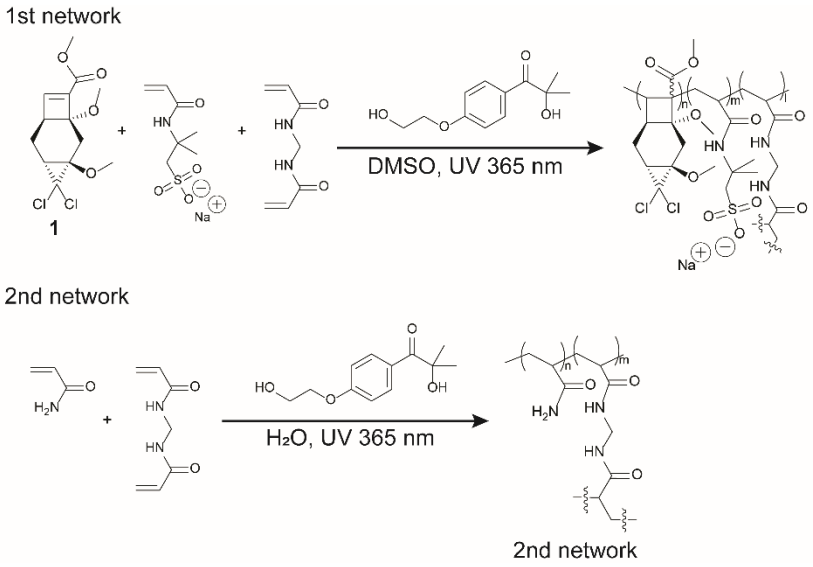

For the synthesis of the single-network (SN) gels, **1**, NaAMPS, and N,N'-methylenebis(acrylamide) (BisAAm) were dissolved in DMSO with vortex and/or sonication (concentration: 0.2 M gated mechanophore, 0.8 M NaAMPS, 6.0 mol% BisAAm). After dissolving all chemicals, 1.0 mol% of 2-Hydroxy-4'-(2-hydroxyethoxy)-2-methylpropiophenone photo initiator was added to the solution (the feed compositions were summarized in Table S2). The mixture was sparged with nitrogen for 5 min, sonicated for 5 min, and brought to a glove bag filled with nitrogen. After staying for 10 min in the glove bag, the solution mixture was poured into a PTFE mold (typical mold size: 3 cm × 3 cm × 1 mm) and covered with a fluorinated glass plate. Then, the mixture was exposed to a 365 nm UV light for 1 day. After curing, the SN was immersed in a DMSO/DI water solution. The DI water content of the solution was gradually increased in order to remove unreacted monomers and to switch the solvent from DMSO to DI water. The gradual shift was as follows, with the SN spending at least 16 h in each solution: DMSO, DMSO/DI water (2:1), DMSO/DI water (1:2), and finally DI water.

For the synthesis of the double-network (DN) gels, the synthesized SN gel was immersed into precursor aqueous solutions for the stretchable second network with the composition of 4.0 M acrylamide (Aam), 0.01 mol% BisAAm, and 0.01 mol% 2-Hydroxy-4'-(2-hydroxyethoxy)-2-methylpropiophenone for 2 days (the precursor solution was exchanged every 24 h). Then, the swollen gel was sandwiched with two glass plates and exposed to a 365 nm UV light for 1 day in a nitrogen glove bag. After the synthesis, the DN gel was immersed in a methyl red sodium salt (MR) aqueous solution (typically 0.3 mM) for the experiments or in a polydimethylsiloxane (PDMS) oil bath to store (if the DN gel was stored in a PDMS oil, it was washed with hexane after taking it out of the oil bath).

Table S2. The formulation of the gels and 1D swelling ratios

1st network					2nd network			
1 (M)	NaAMPS (M)	BisAAm (mol%)	Initiator (mol%)	Swelling ratio in DI water	AAm (M)	BisAAM (mol%)	Initiator (mol%)	Swelling ratio in 0.3 mM MR solution
0.2	0.8	6.0	1.0	2.11	4.0	0.01	0.01	2.42

3. Sonication experiment

3.1. Mechanochemical activation of the mechanophores under sonication

Sonication experiments were conducted using a Sonics Vibracell Model VCX750 at 20 kHz with a 13 mm diameter probe under an ice bath. The amplitude was set as 30%, and the sonication sequence was set as 1 s on and 1 s off. The sonication samples (**2a**) were prepared in THF with the concentration of 2 mg/ml, purged with nitrogen before sonication, and kept under nitrogen atmosphere during the entire experiment. At each time point, an aliquot of the sonicated sample was taken and subjected to GPC analysis to monitor molecular weight as a function of sonication time. To probe HCl release, 0.1 ml of 2 mM rhodamine B base in THF solution was added to 0.9 ml of the sonicated solution. Then, the sonicated solutions were diluted to 1 mg/ml with THF, and UV-vis spectra of these sonicated solutions were collected. The remaining sample solutions were condensed and dried under high vacuum. For the sample with 240 min sonication, the sonicated polymer was precipitated in methanol once to remove byproducts for clear NMR signals and was further dried under high vacuum.

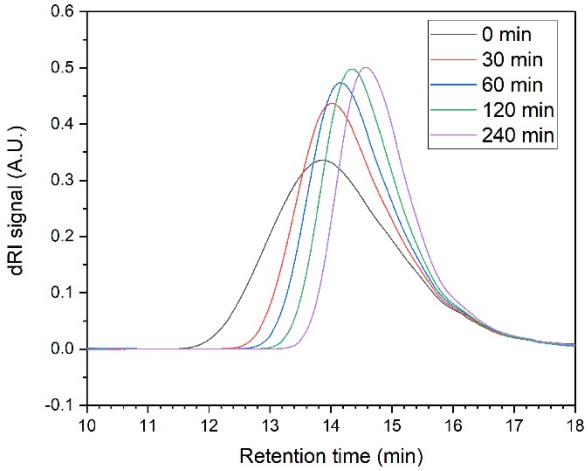

Fig. S10. GPC traces at different sonication times.

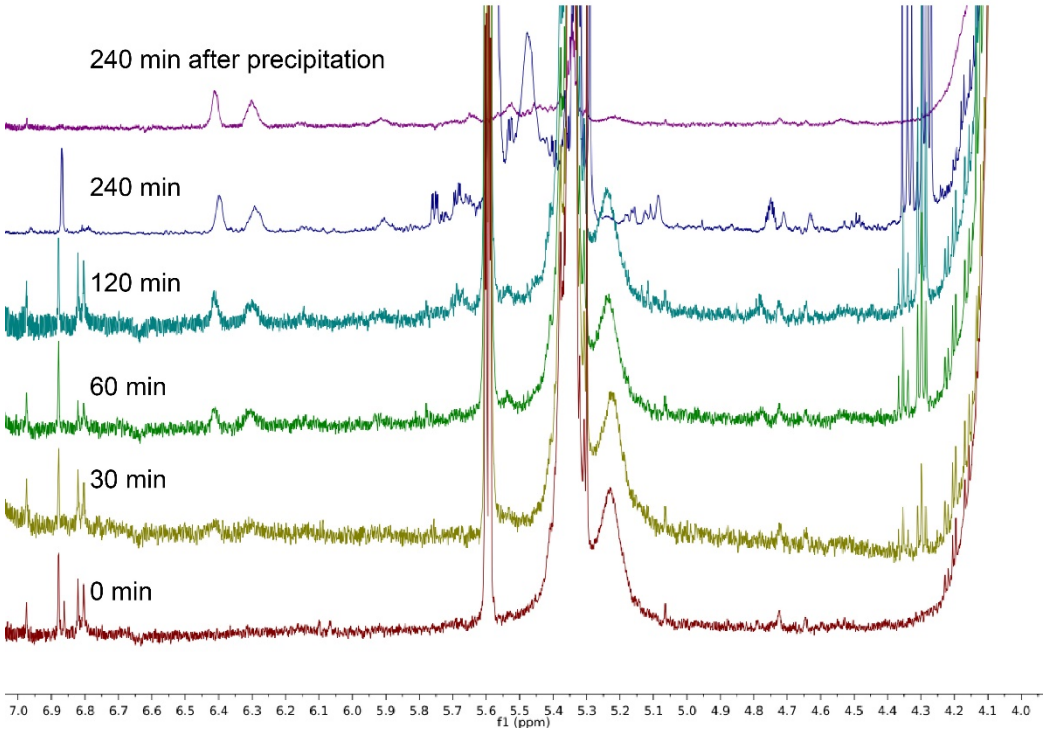

Fig. S11. ^{1}H NMR (500 MHz, $CDCl_3$) spectra at different sonication times.

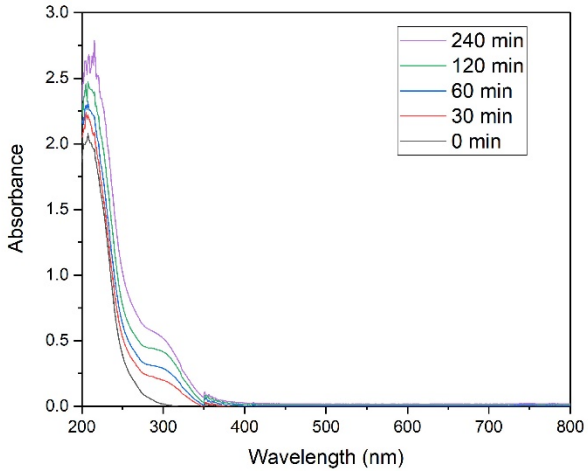

Fig. S12. UV-vis spectra at different sonication times.

3.2. Detection of the released acid by pH indicator

To probe HCl acid release, 0.1 ml of 2 mM rhodamine B base in THF solution was added to 0.9 ml of the sonicated solution. While the unsonicated solution remains colorless, the sonicated solutions show instantaneous color changes to pink. For further analysis, UV-vis measurements were conducted. To get rid of extraneous data caused by the scattering, the absorbance value at 800 nm was subtracted from the entire spectrum.

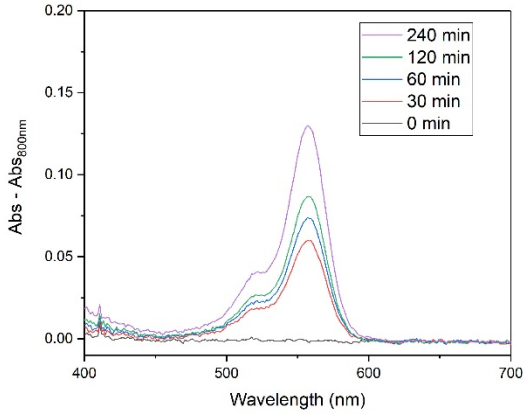

Fig. S13. The UV-vis spectra of the sonicated solutions with rhodamine B base.

4. Single molecule force spectroscopy (SMFS) analysis

SMFS analysis allows for the quantification of polymer extension that occurs due to force-triggered mechanophore activation. For **2b** (**2b'**) before the mechanophore activation (i.e., prior to the plateau feature at ~2 nN), its contour length (L_0) was determined by fitting the regime of the force-separation curve to an extended freely jointed chain (FJC) model, as described previously (Fig. S14a).[2,3] During the mechanochemical reactions, polymer **2b** (**2b'**) detached abruptly from

the probe at a force of ~2.4 nN (Fig. S14b and Table S3). The fact that there is an abrupt post-transition region is a common feature in SMFS experiments for mechanophores with a high transition fore, indicating that at least some but perhaps not all of the gated mechanoacid units were activated prior to detachment from the AFM cantilever. The length of polymer extension (Δx) was estimated by measuring the starting position of the plateau and the detachment position ($\Delta x = x_2 - x_1$ in Fig. S14a), and its percentage of the extra extension (*EE%*) was calculated as $EE\% = \Delta x / L_0 \times 100$. *EE%* ranges from 3.7% to 8.0%, and the fitting results are summarized in Table S3.

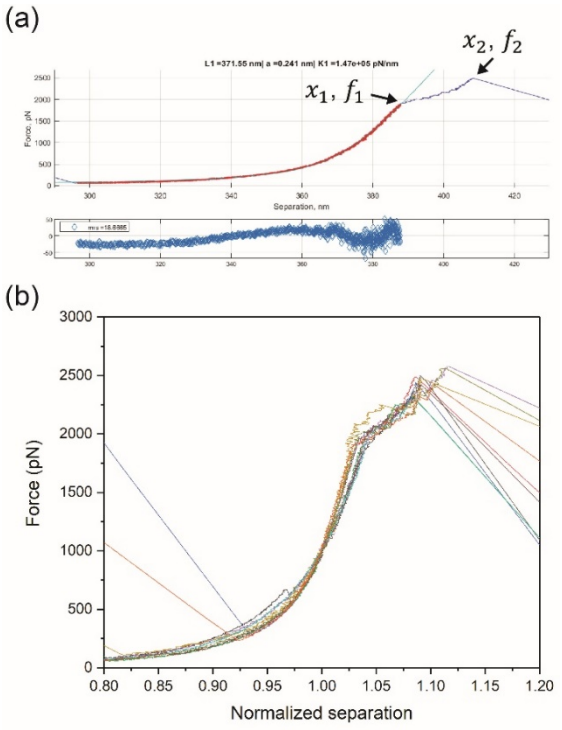

Fig. S14. The results of SMFS analysis: (a) representative SMFS curve fitting and (b) overlayed curves of all the SMFS results. In (a), the red region is the fitted area, and the line with aqua color is the fitting line.

Table S3. Summary of the SMFS fitting and extra extension ratio

ID	L_0 (nm)	Kuhn length (nm)	$k_1 \times 10^5$ (pN/nm)	f^* (pN)	x_1 (nm)	f_1 (pN)	x_2 (nm)	f_2 (pN)	Δx (nm)	$EE\%$
1	558.9	0.200	1.16	2020	594.6	1839	625.3	2490	30.7	5.50
2	371.5	0.241	1.47	2051	388.0	1908	408.6	2486	20.5	5.53
3	536.0	0.233	1.61	2032	559.2	1952	587.8	2424	28.6	5.33
4	528.4	0.255	1.18	2055	562.8	2051	582.2	2320	19.5	3.68
5	182.8	0.207	1.29	2216	195.4	2059	208.1	2575	12.7	6.94
6	194.1	0.148	3.98	2218	198.0	2079	210.3	2464	12.3	6.31
7	518.8	0.222	1.09	2091	553.1	1943	576.6	2304	23.4	4.51
8	469.4	0.233	1.32	2115	494.4	1962	519.0	2413	24.6	5.25
9	224.4	0.212	1.91	2057	233.2	1995	251.2	2562	18.0	8.04
10	297.9	0.219	2.02	2061	307.9	1891	330.2	2423	22.4	7.51

5. CoGEF modeling

Modeling details and the calculation for monomer contour length

The monomer contour lengths (*l*) were calculated using the well-established CoGEF method (constrained geometry simulate external force),[14] and the detailed procedure of how monomer contour lengths are modeled using Spartan® software has been described previously.[3,15] Briefly, the equilibrium conformers of each monomer were first minimized at the molecular mechanics level of theory. The end-to-end distance of the molecule (the distance between blue dots in Fig. S15 and S16) was constrained and extended until the bonding geometries along the direction of pulling were noticeably distorted. Then, its minimized energies at each step were calculated as the end-to-end was shortened in 0.1 Å increments, and CoGEF plots of energy (*E*) as a function of end-to-end distance (*d)* were obtained. The force at the midpoint of the increment (($d_{n+1} + d_n$)/2) was calculated as the slope of the two points (($E_{n+1} - E_n$)/($d_{n+1} - d_n$)) divided by Avogadro constant, and the equilibrium end-to-end distance at force = 0 was determined by extrapolating the force vs. ($d_{n+1} + d_n$)/2 curve to zero force (Fig. S15 and S16). Here, the force ranging from 1 nN to 3 nN was used for the fitting based on the observed activation forces of ~2 nN in the SMFS experiments. Then, the contour length of the monomer was calculated as the average of the distances between the green dots and between the orange dots at force = 0, where the end-to-end distance are the equilibrium end-to-end distance at force = 0 (the green and orange dots are in Fig. S15 and S16).

The contour lengths of the following monomers were calculated: trans-gated mechanoacid, cis-gated mechanoacid, *n*BA, AAEMA, NaAMPS, all potential trans-gated mechanoacid open forms, and all potential cis-gated mechanoacid open forms. For the gated mechanoacid-open forms, we assumed two basic forms (form 1 and 2 in Fig. S16a) based on our previous study on MeO-gDCC based mechanoacid[8,16,17] and calculated all trans (maximum contour length) and all cis (minimum contour length) cases to determine the maximum and the minimum length extension. Data from the calculations are summarized in Fig. S15 and S16 and Table S4.

Calculation for the change in polymer contour length and percent extra extension

The following equations were used to calculate the changes in polymer contour lengths before and after activation (L_F/L_0) and the percentage of extra extension (*EE%*). For the SMFS polymer (**2b**, **2b'**), the incorporation ratios (ϕ) of each monomer were calculated based on the NMR spectrum, and the feeding ratios were used for the incorporation ratios of each monomer in the polymer strand inside the double-network hydrogel. There are 2 cases for the contour length of monomer **1** (l_1: trans-**1** and cis-**1**) and 4 cases for the contour length of the activated forms ($l_{1\ \mathrm{open}}$: each form has its all trans and all cis cases in Fig. S16). Therefore, there will be 8 values of L_F/L_0 and *EE%* for each polymer. The calculated range of the percent extra extension (*EE%*) for the SMFS polymer was 10.3% to 12.9% with $\phi_1 = 0.039$, $\phi_{n\mathrm{BA}} = 0.775$, and $\phi_{\mathrm{AAEMA}} = 0.186$, and the calculated range for the polymer strand inside the DN hydrogel was 52.5% to 65.9% with the $\phi_1 = 0.200$ and $\phi_{\mathrm{NaAMPS}} = 0.800$. The calculated data are summarized in Table S5 and S6.

For the SMFS polymer (2b, 2b')

$$\frac{L_F}{L_0} = \frac{\phi_{\mathbf{1}} \times l_{\mathbf{1}\,open} + \phi_{nBA} \times l_{nBA} + \phi_{AAEMA} \times l_{AAEMA}}{\phi_{\mathbf{1}} \times l_{\mathbf{1}} + \phi_{nBA} \times l_{nBA} + \phi_{AAEMA} \times l_{AAEMA}}$$

For the polymer strand polymer inside the double-network hydrogel

$$\frac{L_F}{L_0} = \frac{\phi_{\mathbf{1}} \times l_{\mathbf{1}\,open} + \phi_{NaAMPS} \times l_{NaAMPS}}{\phi_{\mathbf{1}} \times l_{\mathbf{1}} + \phi_{NaAMPS} \times l_{NaAMPS}}$$

The percentage of the extra extension ($EE\%$)

$$EE\% = \left(\frac{L_F}{L_0} - 1\right) \times 100$$

Table S4. The contour lengths of monomers

	1		***n*BA**	**AAEMA**	**NaAMPS**	**Open form 1**		**Open form 2**	
	trans	cis				trans	cis	trans	cis
Contour length (Å)	2.67	2.70	2.53	2.55	2.54	11.13	9.46	11.05	9.49

Table S5. The estimated change in the polymer contour length before and after mechanophore activations

		SMFS Polymer (2b)				**Strand in the DN hydrogel**			
		Open form1		Open form 2		Open form1		Open form 2	
		trans (max)	cis (min)	trans (max)	cis (min)	trans (max)	cis (min)	trans (max)	cis (min)
$\frac{L_F}{L_0}$	L_0: based on trans-1	1.13	1.10	1.13	1.10	1.66	1.53	1.65	1.53
	L_0: based on cis-1	1.13	1.10	1.13	1.10	1.66	1.53	1.65	1.53

Table S6. The estimated percentage of extra extension

		SMFS Polymer (2b)				**Strand in the DN hydrogel**			
		Open form1		Open form 2		Open form1		Open form 2	
		trans (max)	cis (min)	trans (max)	cis (min)	trans (max)	cis (min)	trans (max)	cis (min)
EE%	L_0: based on trans-1	12.9	10.4	12.8	10.4	65.9	52.9	65.3	53.2
	L_0: based on cis-1	12.9	10.3	12.8	10.4	65.5	52.5	64.9	52.8

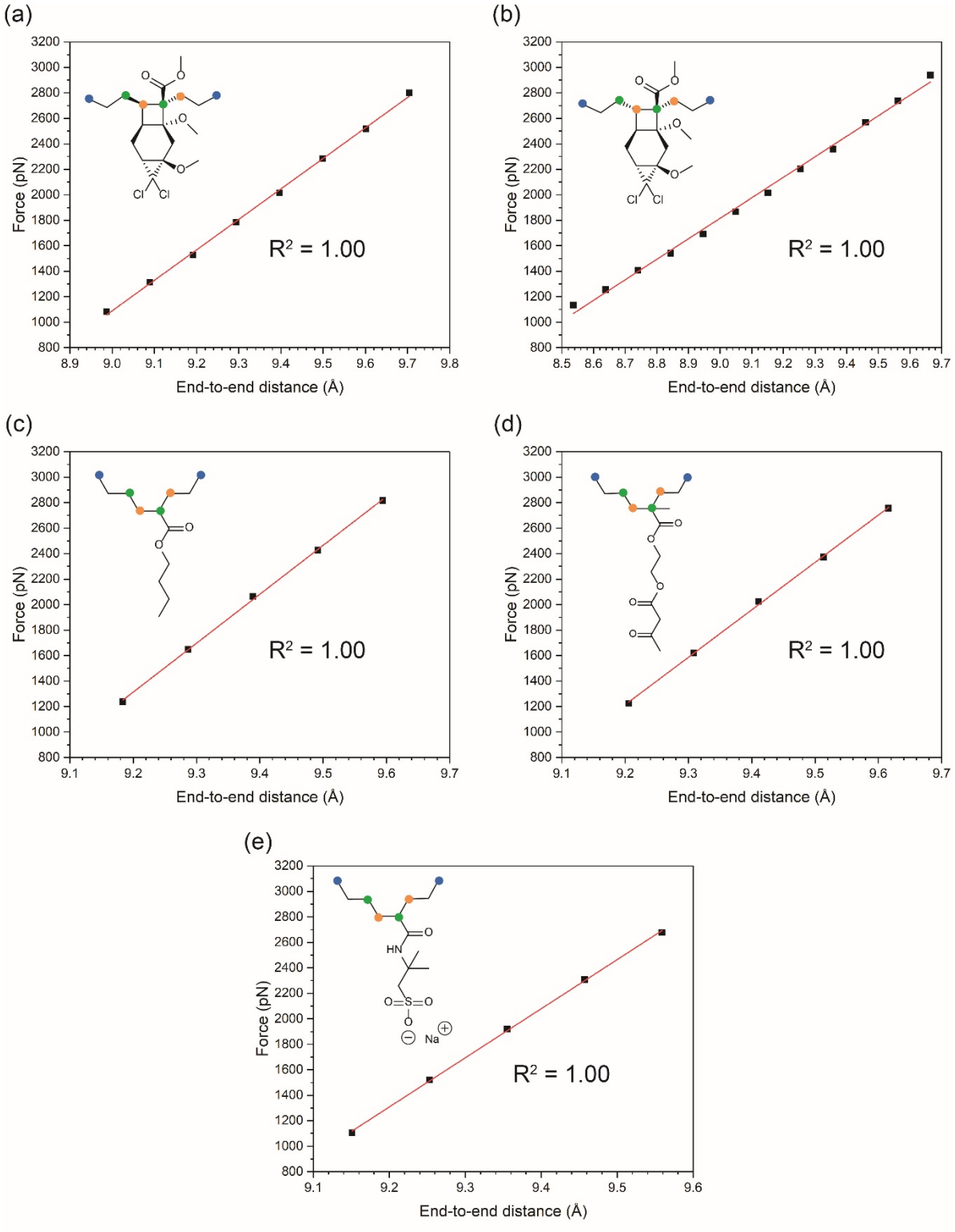

Fig. S15. Force vs. displacement curves of non-mechanophore monomers obtained by CoGEF: (a) trans-**1**, (b) cis-**1**, (c) *n*BA, (d) AAEMA, and (e) NaAMPS. The red lines are the linear fitting curves.

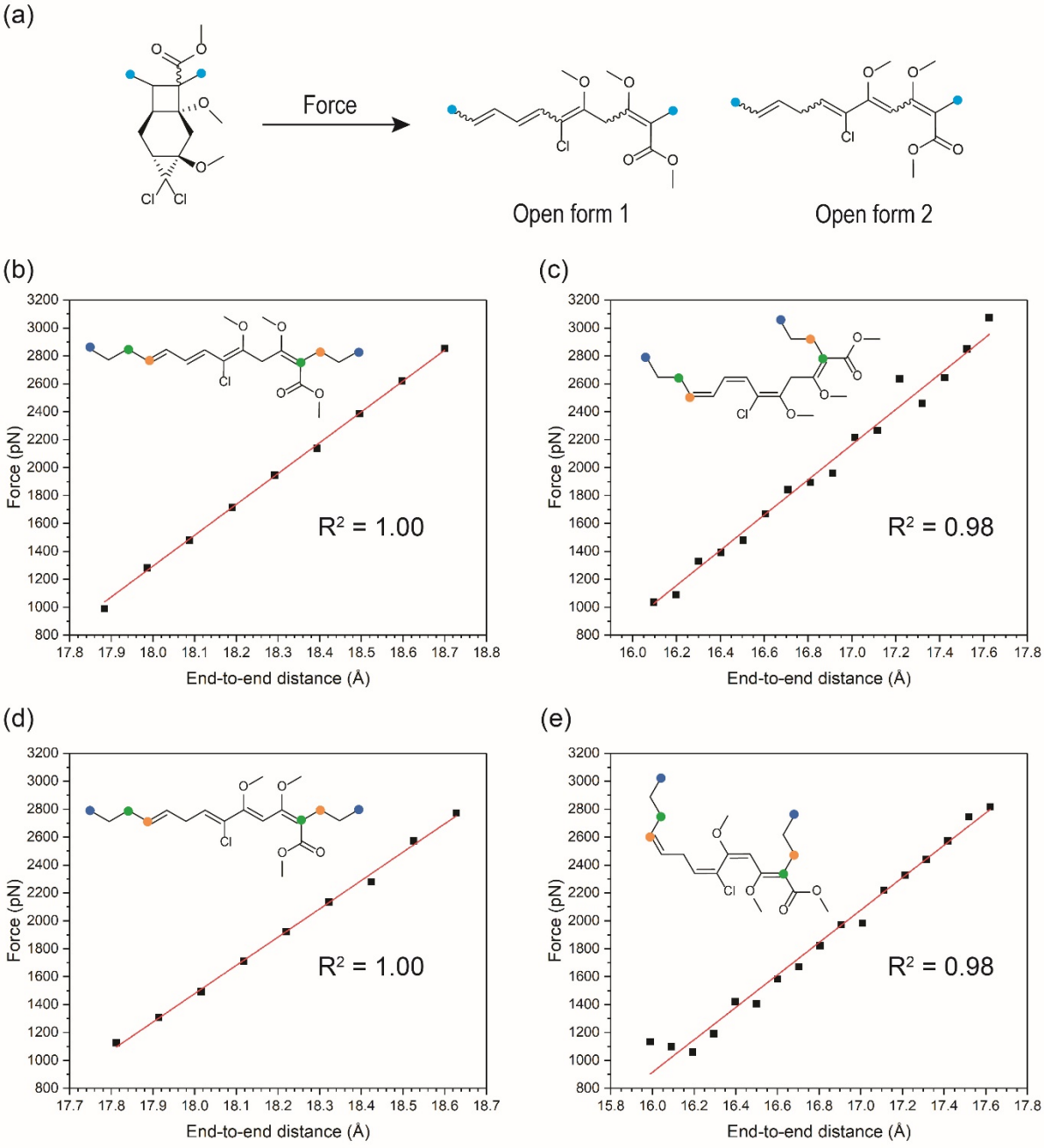

Fig. S16. Force vs. displacement curves of gated mechanoacid monomers obtained by CoGEF: (a) anticipated product structures, (b) trans-open form 1, (c) cis-open form 1, (d) trans-open form 2, and (e) cis-open form 2. The red lines are the linear fitting curves.

6. Analysis of double-network hydrogels

6.1. Image analysis during tensile testing

Image analysis was conducted with a similar procedure to previous methods.[18–20] The images were taken using a Canon EOS RebelTM xsi with a Cannon EF-S 18-55 mm f/3.5-5.6 IS SLR lens. The manual mode was used with the setting of exposure time 1/4 sec, F-stop f/5.6, ISO speed ISO-100. The camera settings and its position were fixed for the entire duration of the tensile tests. The files were saved as CR2 format and imported into Adobe Lightroom Classic CC software, where white balance function was applied to all images to standardize. The files were exported as TIFF files and imported into Fiji image J software for further image analysis. Then, each image file was split into red, green, and blue channels, and mean pixel intensities of each channel in non-necking area, necking area, and area representing the whole sample were recorded. For the area representing the whole sample, the rectangular area, which was within the sample but covered an area between grips, was chosen. For each picture, the strain was calculated by measuring the distances between the two grips: $\varepsilon = \frac{Current\ length - Initial\ length}{Initial\ length}$.

The results of the image analysis are summarized in Fig. S17. Initially, R, G, and B ratios (R/(R+G+B), G/(R+G+B), B/(R+G+B)) in the area representing the whole sample closely follow those in the non-necking area. However, around the yield point, the necking area starts to appear, and the ratios in the area representing the whole sample start to deviate from those in the non-necking area. Then, the curves move towards the curves for the necking area and finally almost overlap around the point where the entire sample yields and starts to show strain hardening. The data quantitatively confirm that the acid release due to the mechanochemical reactions followed by the acid-base reaction happens in the necking region which propagates to the entire sample as the strain increases.

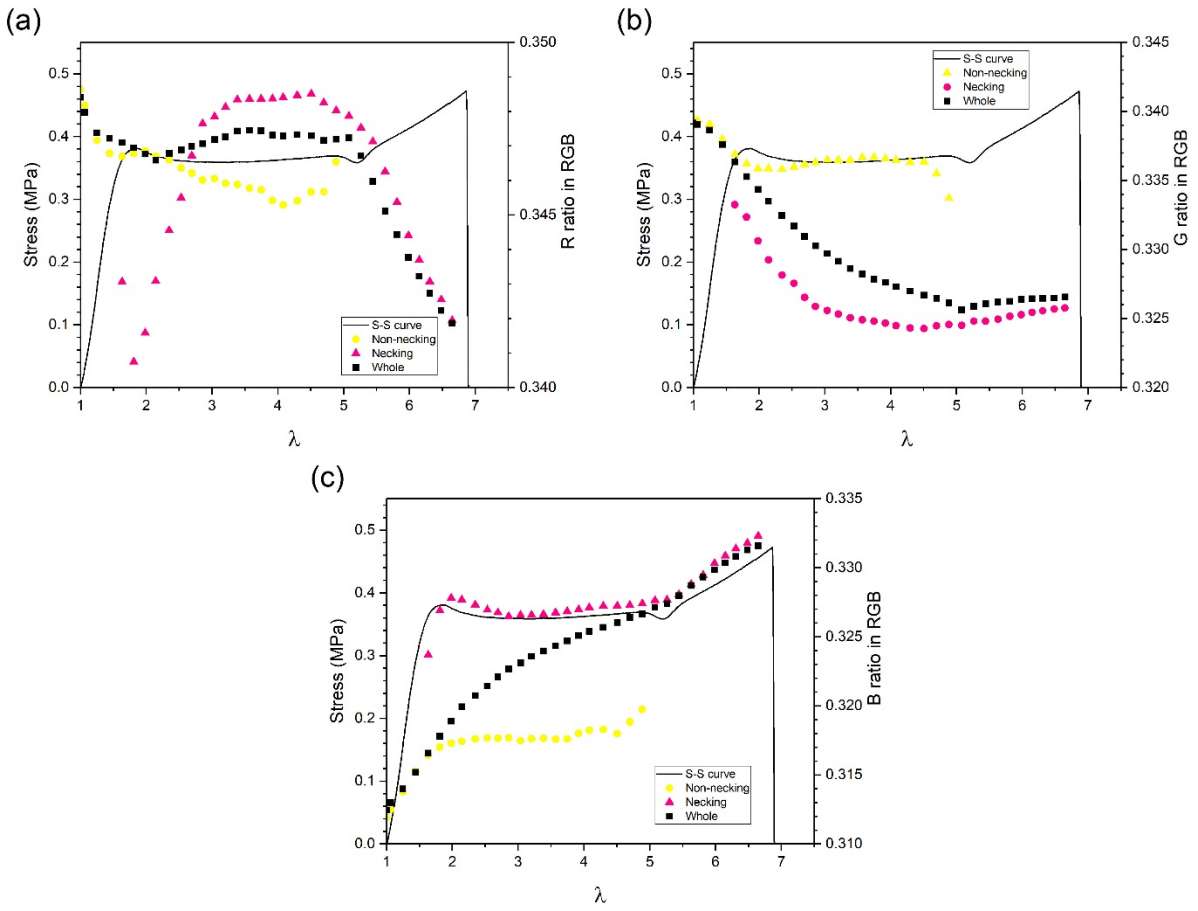

Fig. S17. RGB image analysis during the tensile test: (a) R ratio in the total RGB, (b) G ratio in the total RGB, and (c) B ratio in the total RGB.

6.2. pH measurements and mechanophore activation ratios inside the double-network hydrogels

6.2.1. Calibration for pH measurements

To make a calibration curve, the attenuation coefficient of the methyl red (MR) was determined inside the pre-gel solution environments. The composition of the pre-gel solutions was calculated based on the feeding ratio and the swelling ratio of the DN hydrogel and is summarized in Table S7 (the gated mechanoacid portion was replaced with DI water due to its solubility issue in DI water, and the initiator was excluded to avoid polymerization inside a cuvette). The attenuation coefficient at the isosbestic point (472 nm) was determined to be 15512 $M^{-1}cm^{-1}$ with the R^2 value close to 1 (Fig. S18).

For the pH calibration curve, the concentration of MR inside the DN hydrogel was measured to be 2.9×10^{-5} M based on the UV-vis absorbances of the DN hydrogels at the isosbestic point (472 nm), and the pre-gel solution with the measured concentration of MR was prepared. To the pre-gel solution, HCl was introduced, and its pH and UV-vis spectrum were measured to obtain the calibration curve (Fig. S19). For the attenuation coefficient and pH calibration, the UV-vis spectra were corrected by subtracting the absorbance values at 635 nm from the entire spectra to

minimize the effects of scattering (i.e., $Abs - Abs_{635\ nm}$). The effects of scattering become larger as the wavelength becomes shorter, and the absorbance at the minimum wavelength below which the absorbance peak of protonated MR starts (around 530 nm) to appear is the largest absorbance originating only from the scattering. Therefore, the absorbance at 635 nm was chosen as the constant value to subtract based on Fig. S19a. The peak ratios of protonated MR at 530 nm to unprotonated MR at 440 nm ($Abs_{530\ nm}/Abs_{440\ nm}$) were calculated at each pH to construct the pH calibration curve (Fig. S19b).

Table S7. The formulation of the pre-gel solution and the swelling ratios for the attenuation coefficient measurement and the pH calibration curve (the swelling ratios are based on 1D).

Swelling ratio		Concentration		
1st network in the 2nd network pregel solution	DN hydrogel in 0.3 mM MR solution	NaAMPS	BisAAm	AAm
2.10	2.42	56.4 mM	4.49 mM	2.62 M

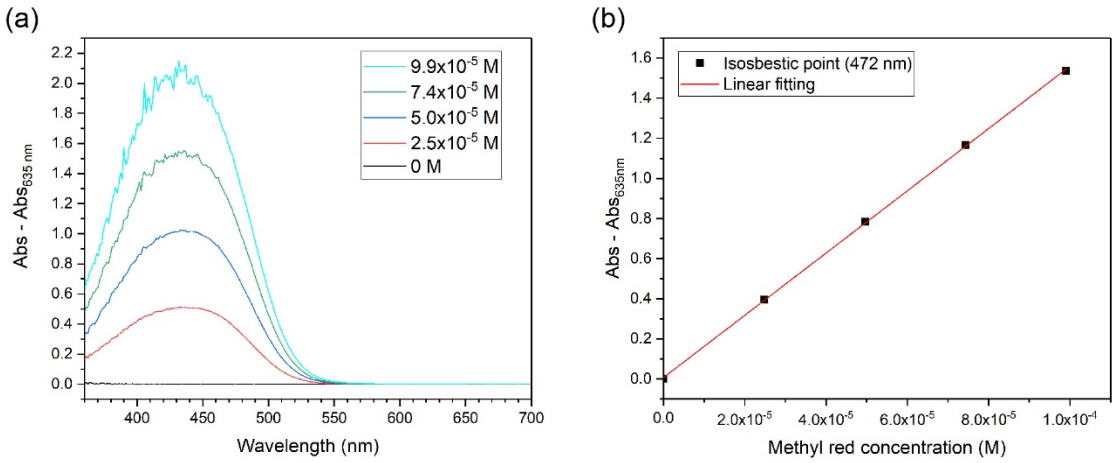

Fig. S18. The UV-vis results of the pre-gel solutions with different MR concentrations: (a) the UV-vis spectra and (b) the absorbance at the isosbestic point (472 nm) with different MR concentrations. The slope (attenuation coefficient) and intercept of the linear fitting are 15512 $M^{-1}cm^{-1}$ and 0.0072, respectively, with $R^2 = 0.9998$.

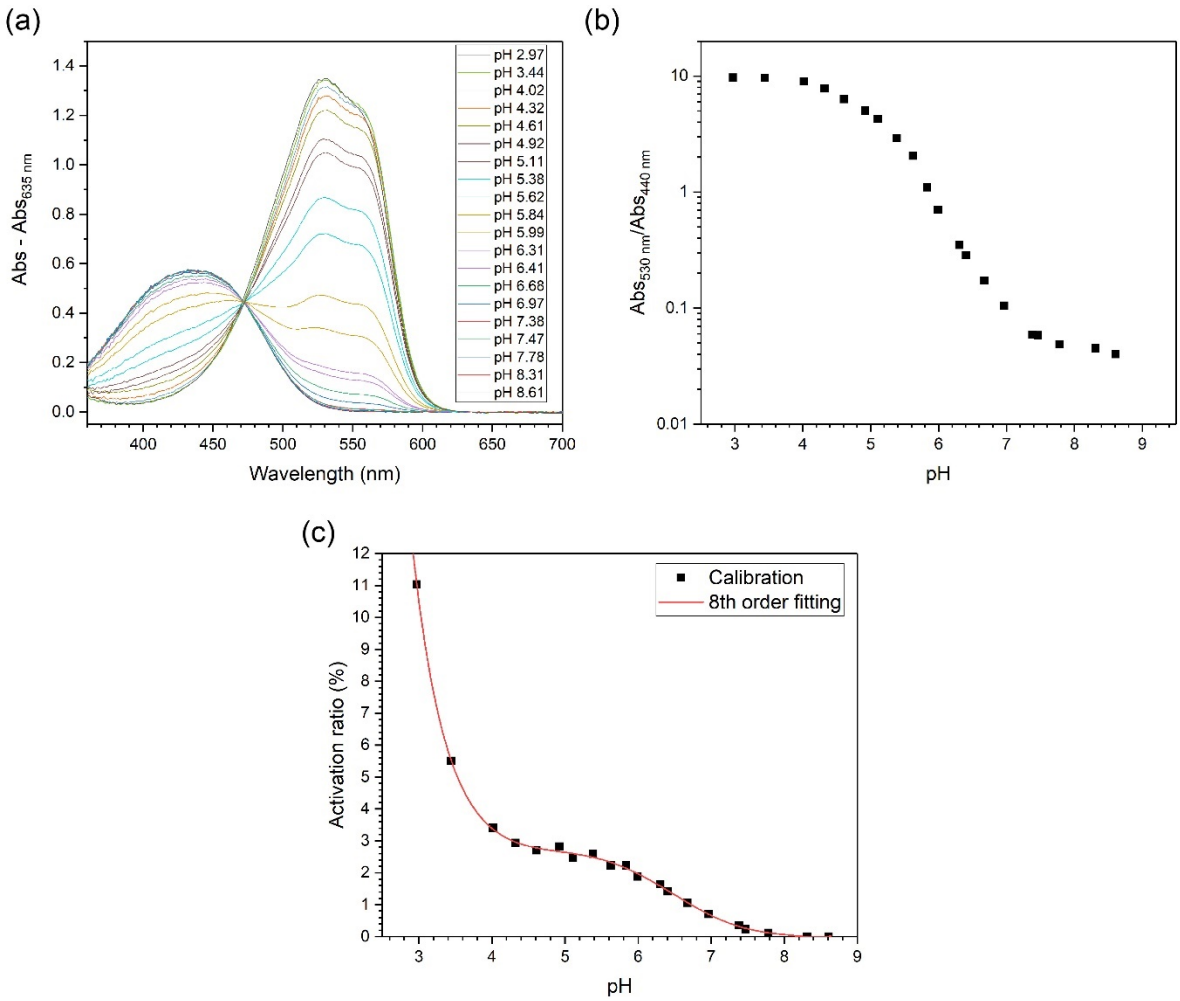

Fig. S19. Calibrations for pH and mechanophore activation measurements: (a) UV-vis spectra with different pH, (b) the calibration curve for pH, and (c) the calibration curve for the activation ratio of the mechanophore.

6.2.2. The processing of the UV-vis spectra to minimize scattering effects

The pH inside the DN hydrogels was measured based on the UV-vis spectra and the calibration curve. For the samples after mechanical loadings, the following two methods were applied to minimize the effects of scattering in the UV-vis spectra (Fig. S20 and S21): (i) Subtracting the fitting function based on scattering and (ii) Subtracting the constant absorbance at 635 nm ($Abs - Abs_{635\ nm}$). For the sample before mechanical loadings, only method (ii) was applied. After the correction of the spectra, the peak ratios of protonated MR at 530 nm to unprotonated MR at 440 nm were calculated, and the pH was determined by interpolating the calibration curve (Fig. S19b and Table S8).

(i) Subtracting the fitting function based on scattering

The UV-vis spectra were corrected by subtracting the following fitting function which takes scattering effects into account (Fig. S20). The two regions around both edges of the protonated MR peak around 530 nm were used to achieve a reliable fitting: from 360 nm to 380 nm and from 640 nm to 700 nm.

$$Abs_{scattering} = \log\left(\frac{1}{1 - c\lambda^{-4}}\right) + A_0$$

c and A_0 are fitting constants, and λ is wavelength.

Although the region from 360 nm to 380 nm is supposed to be slightly higher than 0, this method makes this region almost 0. Therefore, the corrected absorbance value for unprotonated MR around 440 nm becomes smaller than the real value, thus the calculated pH value is considered to slightly underestimate the true pH value (i.e., minimum pH).

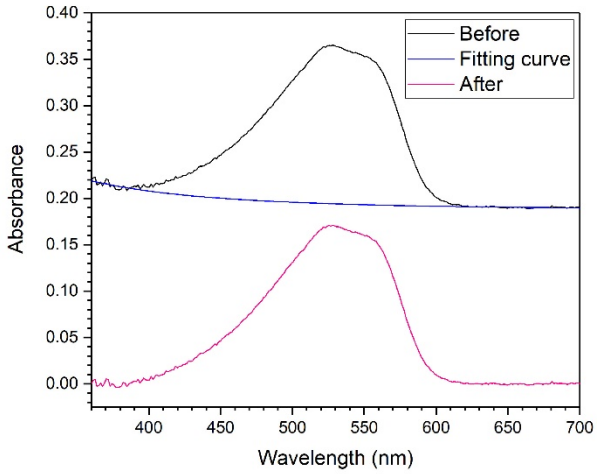

Fig. S20. The correction of UV-vis spectrum with the fitting function taking scattering effects into account. A representative spectrum after mechanical loadings.

(ii) Subtracting the constant absorbance at 635 nm

The UV-vis spectra were corrected by subtracting the absorbance values at 635 nm from the entire spectra to minimize the effects of scattering ($Abs - Abs_{635\ nm}$ in Fig. S21). The effects of scattering become larger as the wavelength becomes shorter, and the absorbance at the minimum wavelength below which the absorbance peak of protonated MR (around 530 nm) starts to appear is the largest absorbance originating only from the scattering. Therefore, the absorbance at 635 nm was chosen as the constant value to subtract based on Fig. S19a. Since absorbances at wavelengths lower than 635 nm contain more scattering effects, the real absorbances of unprotonated MR around 440 nm is smaller than $Abs_{440\ nm} - Abs_{635\ nm}$. Therefore, the calculated pH after mechanical loading is overestimated and represents maximum pH.

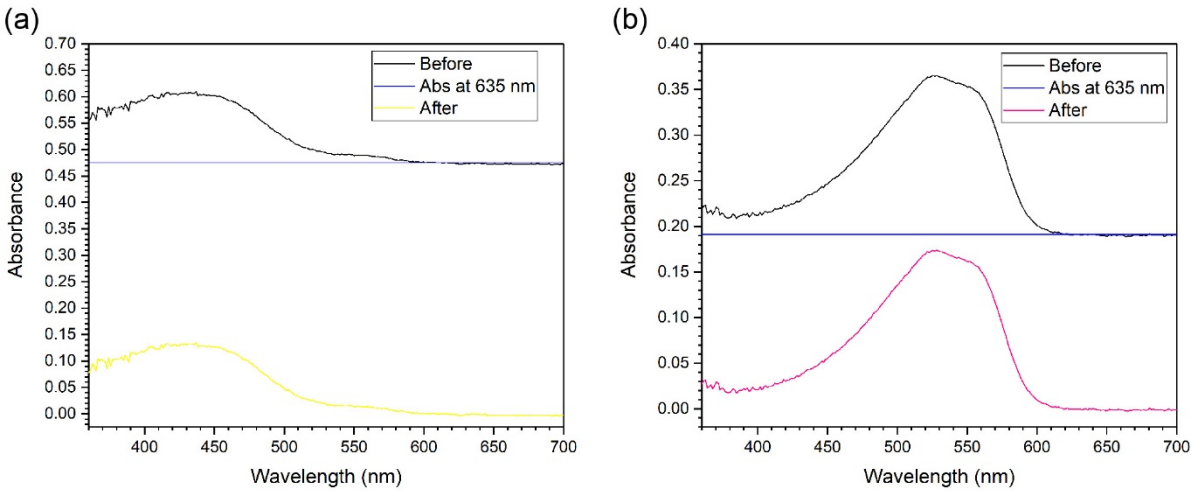

Fig. S21. The correction of UV-vis spectra by subtracting constant absorbance value at 635 nm: representative spectra (a) before mechanical loadings and (b) after mechanical loadings.

6.2.3. The summary of the pH values inside the double-network hydrogels

The DN hydrogels were immersed in 0.3 mM MR aqueous solutions. After taking these gels out of the MR solution, mechanical loadings were applied: a DN hydrogel was struck multiple (~60) times with a hammer (DN-1 to DN-4) or stretched until it broke with a custom-made stretcher (DN-stretch). The UV-vis spectra before and after mechanical loadings were taken, and the pHs were calculated based on the calibration curve after the UV-vis data processing. To increase the range of pH change, the initial pH inside several DN hydrogels was adjusted by using slightly basic MR aqueous solutions containing NaOH. The pH values of the DN hydrogels calculated by the above methods and the UV-vis spectra are summarized in Table S8 and Fig. S22.

Table S8. Summary of pH before and after mechanical loadings.

Sample ID	MR solution used	pH		
		Before mechanical loading	After mechanical loading	
		$Abs - Abs_{635\ nm}$	$Abs - Abs_{\ scattering}$ (min)	$Abs - Abs_{635\ nm}$ (max)
DN-1	MR 0.3 mM (No NaOH)	6.76	4.96	5.23
DN-2	MR 0.3 mM (No NaOH)	7.36	5.21	5.45
DN-3	MR 0.3 mM with pH 8	6.68	5.02	5.15
DN-4	MR 0.3 mM with pH 9	7.26	5.23	5.43
DN-stretch	MR 0.3 mM (No NaOH)	6.36	5.59	5.76

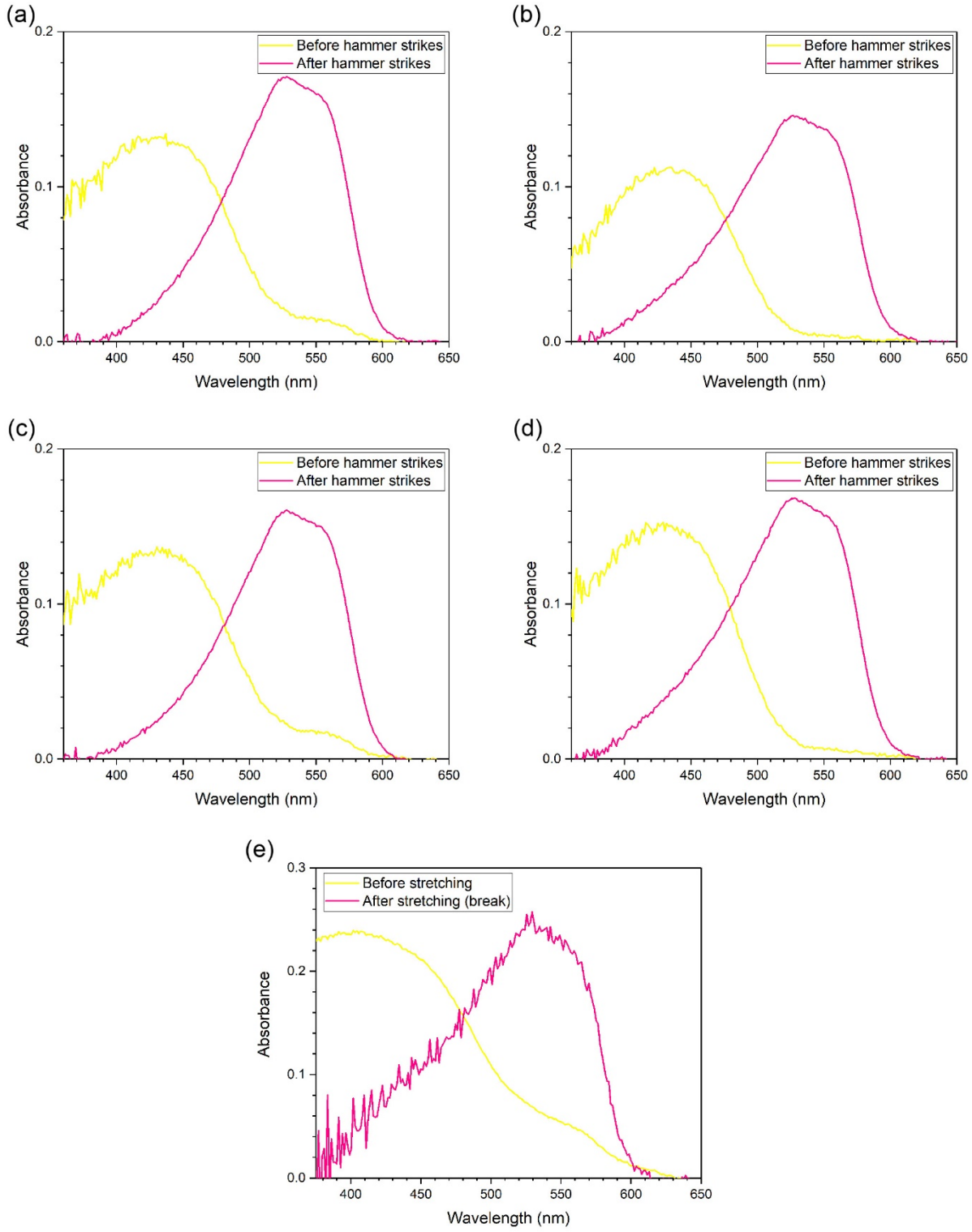

Fig. S22. Representative UV-vis spectra before and after mechanical loadings: (a) DN-1 (No NaOH), (b) DN-2 (No NaOH), (c) DN-3 (pH 8), (d) DN-4 (pH 9), and (e) DN-stretch. DN-1 to DN-4 were struck multiple times with a hammer, and DN-stretch was uniaxially stretched with a custom-made stretcher. The UV-vis spectra were processed to minimize the effects of scattering:

the spectra before mechanical loadings were corrected by subtracting the constant absorbance value at 635 nm from the spectra, while those of after mechanical loadings are the corrected absorbance spectra with fitting function taking scattering effects into account.

6.2.4. The control experiments for the acidification inside double-network hydrogels

The control experimets were conducted with the following procedures. The control DN hydrogel (without monomer **1**) was synthesized with the same procedure as the DN hydrogel with monomer **1** except for the monomer composition. 1.0 M NaAMPS, 6.0 mol% BisAAm, and 1.0 mol% 2-Hydroxy-4'-(2-hydroxyethoxy)-2-methylpropiophenone photo initiator were used for the single network, and 4.0 M acrylamide, 0.01 mol% BisAAm, and 0.01 mol% 2-Hydroxy-4'-(2-hydroxyethoxy)-2-methylpropiophenone were chosen for the second network. After the fabrication, the control DN hydrogel was immersed in an aqueous solution of 14.1 mM of control mechanoacid molecule (molecule **2**), which is the same concentration as that of monomer **1** in the DN hydrogel with monomer **1**, and 0.51 mM of MR pH indicator over 16 h (the MR concentration was adjusted to make MR concentration inside the control DN hydrogel within 15% difference compared to that inside the DN hydrogel with monomer **1**). After taking the control DN hydrogel out of the solution, mechanical loadings were applied: the DN-control hydrogel was struck multiple (~60) times with a hammer. The UV-vis spectra before and after mechanical loadings were taken, and the pHs were calculated based on the calibration curve after the UV-vis data processing (i.e., subtracting the constant absorbance value at 635 nm from the spectra). The control DN sample shows no obvious color change before and after hammer strikes (Fig. S23). Therefore, almost no pH change is observed: pH before hammer strikes is 6.44, while that of after hammer strikes is 6.60.

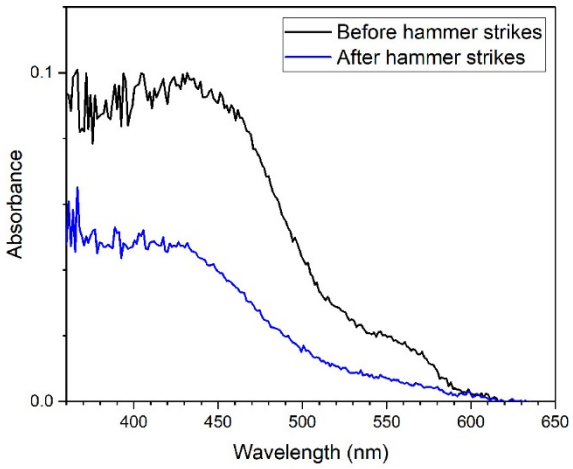

Fig. S23. Representative UV-vis spectra of the control DN hydrogel before and after mechanical loadings: The UV-vis spectra were processed to minimize the effects of scattering by subtracting the constant absorbance value at 635 nm from the spectra.

6.2.5. Mechanophore activation ratios inside the DN hydrogels.

To measure the activation ratio of the gated mechanoacid inside the DN gel, the calibration curve of the activation ratio against pH was constructed (Fig. S19c). Based on the initial feeding ratio of the gated mechanoacid (0.2 M) and the swelling ratio (2.42), the maximum HCl concentration (i.e., 100% mechanophore activation) was calculated as 0.014 M. During the titration for Fig. S19a and b, the activation ratio was calculated as $\frac{Total\ amount\ of\ HCl\ added}{Total\ volume\ of\ the\ pregel\ solution \times 0.014} \times 100$ (%), while measuring the pH of the pregel solution. The calibration points were fitted with an 8th order polynominal fitting. The activation ratios before and after mechanical loadings were estimated based on this fitting curve, and the activation ratio induced only by mechanical loading was calculated by subtracting the activation ratio before mechanical loadings from that after mechanical loadings and are summaried in Table S9.

Table S9. Summary of activation ratio before and after mechanical loadings.

Sample ID	Activation ratio (%)	
	$Abs - Abs_{\_scattering}$ (max)	$Abs - Abs_{635\ nm}$ (min)
DN-1 (hammer)	1.70	1.60
DN-stretch	0.83	0.70

6.3. Thermal stability analysis

The thermal stability of the DN hydrogels incorporating monomer **1** was analyzed by measuring UV-vis spectra and pH (Table S10 and S11 and Fig. S24 and S25). After the fabrication, the DN samples were immersed in 0.3 mM MR in DI water solution for a certain period at room temperature (~20 ℃) or 44 ℃. Then UV-vis spectra before and after hammer strikes were measured. For both cases, the MR solutions were occasionally replaced before UV-vis measurements to keep the MR solutions fresh. For the 44 ℃ case, the color change and the corresponding pH drop become less as time passes (Fig. S25 and Table S11) presumably because of the degradation of the DN hydrogels (e.g., hydrolysis of the amide crosslinker in a basic MR solution). However, at room temperature, the DN hydrogel presents a distinct color change from yellow to pink and a pH drop to about 5 even after 28 days (Fig. S24e and f, Table S10). These results confirm that the gated mechanoacid is thermally stable enough to show mechanochemical activation at least after 28 days at room temperature.

Table S10. pH values of the DN hydrogels immersed in MR solution at room temperature (20 ℃).

Period immersed in 0.3 mM MR solution	pH		
	Before hammer strikes	After hammer strikes	
	$Abs - Abs_{635\ nm}$	$Abs - Abs_{\ scattering}$ (min)	$Abs - Abs_{635\ nm}$ (max)
1 day	6.22	5.21	5.59
3 days	6.55	5.15	5.51
7 days	6.40	5.14	5.47
17 days	6.32	5.03	5.39
28 days	6.59	5.16	5.50

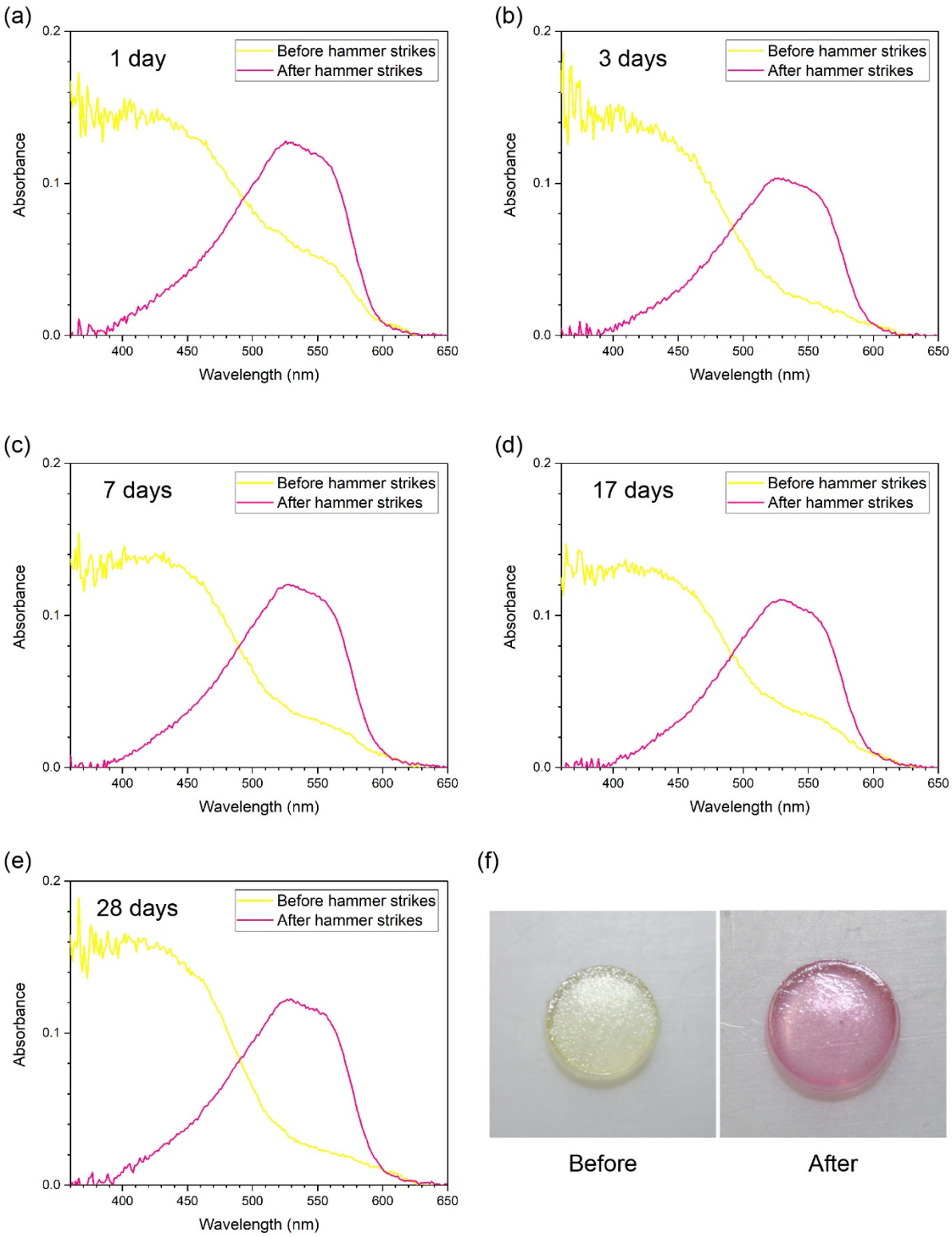

Fig. S24. Thermal stability analysis at room temperature (20 °C): the representative UV-vis spectra before and after hammer strikes (a) after 1 day, (b) after 3 days, (c) after 7 days, (d) after 17 days, and (e) after 28 days, and (f) after 28 day's sample before and after hammer strikes.

Table S11. pH values of the DN hydrogels immersed in MR solution at 44 °C.

Period immersed in 0.3 mM MR solution	pH		
	Before hammer strikes	After hammer strikes	
	$Abs - Abs_{635\ nm}$	$Abs - Abs_{\ scattering}$ (min)	$Abs - Abs_{635\ nm}$ (max)
0 day	6.64	5.22	5.61
3 days	6.60	5.79	5.97
7 days	6.50	6.10	6.26

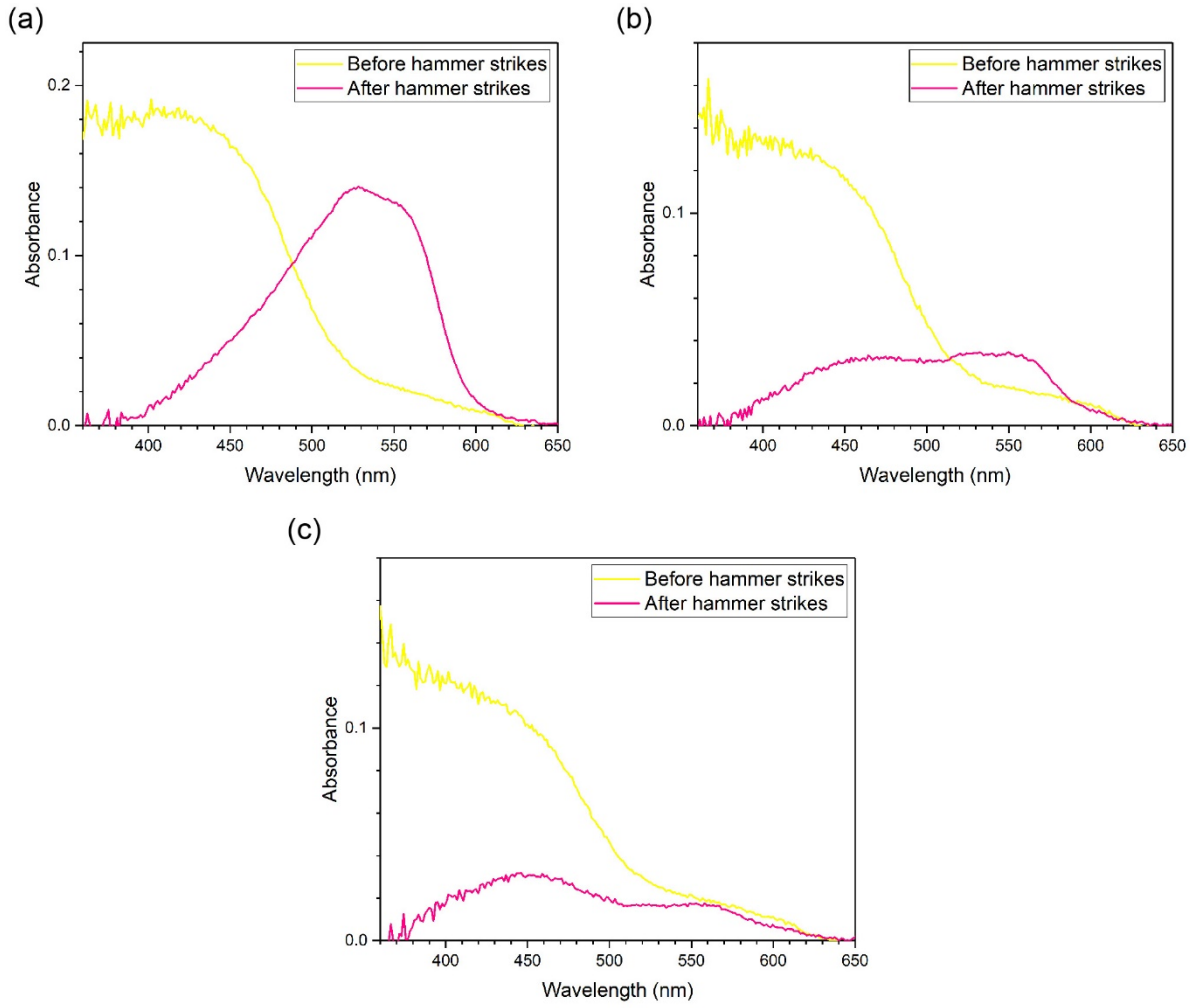

Fig. S25. Thermal stability analysis at 44 °C: the representative UV-vis spectra before and after hammer strikes (a) 0 day, (b) 3 days, and (c) 7 days.

Refences

1 A. F. Oberhauser, P. E. Marszalek, H. P. Erickson and J. M. Fernandez, *Nature*, 1998, **393**, 181.

2 D. Wu, J. M. Lenhardt, A. L. Black, B. B. Akhremitchev and S. L. Craig, *J. Am. Chem. Soc.*, 2010, **132**, 15936–15938.

3 H. M. Klukovich, T. B. Kouznetsova, Z. S. Kean, J. M. Lenhardt and S. L. Craig, *Nat. Chem.*, 2013, **5**, 110–114.

4 J. Wang, T. B. Kouznetsova, Z. Niu, M. T. Ong, H. M. Klukovich, A. L. Rheingold, T. J. Martinez and S. L. Craig, *Nat. Chem.*, 2015, **7**, 323–327.

5 J. Wang, T. B. Kouznetsova, Z. Niu, A. L. Rheingold and S. L. Craig, *J. Org. Chem.*, 2015, **80**, 11895–11898.

6 T. B. Kouznetsova, J. Wang and S. L. Craig, *ChemPhysChem*, 2017, **18**, 1486–1489.

7 E. L. Florin, M. Rief, H. Lehmann, M. Ludwig, C. Dornmair, V. T. Moy and H. E. Gaub, *Biosens. Bioelectron.*, 1995, **10**, 895–901.

8 Y. Lin, T. B. Kouznetsova and S. L. Craig, *J. Am. Chem. Soc.*, 2020, **142**, 99–103.

9 Q. W. Song, B. Yu, A. H. Liu, Y. He, Z. Z. Yang, Z. F. Diao, Q. C. Song, X. D. Li and L. N. He, *RSC Adv.*, 2013, **3**, 19009–19014.

10 B. H. Bowser, C. H. Ho and S. L. Craig, *Macromolecules*, 2019, **52**, 9032–9038.

11 Z. Wang, X. Zheng, T. Ouchi, T. B. Kouznetsova, H. K. Beech, S. Av-Ron, T. Matsuda, B. H. Bowser, S. Wang, J. A. Johnson, J. A. Kalow, B. D. Olsen, J. P. Gong, M. Rubinstein and S. L. Craig, *Science*, 2021, **374**, 193.

12 B. B. Snider, D. J. Rodini, R. S. E. Conn and S. Sealfon, *J. Am. Chem. Soc.*, 1979, **101**, 5283–5293.

13 J. J. Lessard, G. M. Scheutz, S. H. Sung, K. A. Lantz, T. H. Epps and B. S. Sumerlin, *J. Am. Chem. Soc.*, 2020, **142**, 283–289.

14 M. K. Beyer, *J. Chem. Phys.*, 2000, **112**, 7307–7312.

15 B. H. Bowser, S. Wang, T. B. Kouznetsova, H. K. Beech, B. D. Olsen, M. Rubinstein and S. L. Craig, *J. Am. Chem. Soc.*, 2021, **143**, 5269–5276.

16 E. E. Schweizer and W. E. Parham, *J. Am. Chem. Soc.*, 1960, **82**, 4085–4087.

17 S. M. McElvain and P. L. Weyna, *J. Am. Chem. Soc.*, 1959, **81**, 2579–2588.

18 M. H. Barbee, K. Mondal, J. Z. Deng, V. Bharambe, T. V. Neumann, J. J. Adams, N. Boechler, M. D. Dickey and S. L. Craig, *ACS Appl. Mater. Interfaces*, 2018, **10**, 29918–29924.

19 Y. Lin, M. H. Barbee, C. C. Chang and S. L. Craig, *J. Am. Chem. Soc.*, 2018, **140**, 15969–15975.

20 G. R. Gossweiler, G. B. Hewage, G. Soriano, Q. Wang, G. W. Welshofer, X. Zhao and S. L. Craig, *ACS Macro Lett.*, 2014, **3**, 216–219.